A Diffusion Model for Regular Time Series Generation from Irregular Data with Completion and Masking

Gal Fadlon* **Idan Arbiv*** **Nimrod Berman** **Omri Azencot**
Department of Computer Science
Ben-Gurion University of The Negev
{galfad, arbivid, bermann}@post.bgu.ac.il
azencot@cs.bgu.ac.il

Abstract

Generating realistic time series data is critical for applications in healthcare, finance, and science. However, irregular sampling and missing values present significant challenges. While prior methods address these irregularities, they often yield sub-optimal results and incur high computational costs. Recent advances in regular time series generation, such as the diffusion-based ImagenTime model, demonstrate strong, fast, and scalable generative capabilities by transforming time series into image representations, making them a promising solution. However, extending ImagenTime to irregular sequences using simple masking introduces "unnatural" neighborhoods, where missing values replaced by zeros disrupt the learning process. To overcome this, we propose a novel two-step framework: first, a Time Series Transformer completes irregular sequences, creating natural neighborhoods; second, a vision-based diffusion model with masking minimizes dependence on the completed values. This approach leverages the strengths of both completion and masking, enabling robust and efficient generation of realistic time series. Our method achieves state-of-the-art performance, achieving a relative improvement in discriminative score by 70% and in computational cost by 85%. [Code is at https://github.com/azencot-group/ImagenI2R]

1 Introduction

Time series data is essential in fields such as healthcare, finance, and science, supporting critical tasks like forecasting trends, detecting anomalies, and analyzing patterns [14, 20, 30]. Beyond direct analysis, generating synthetic time series has become increasingly valuable for creating realistic proxies of private data, testing systems under new scenarios, exploring "what-if" questions, and balancing datasets for training machine learning models [3]. The ability to generate realistic sequences enables deeper insights and robust applications across diverse domains.

In practice, however, time series data is often *irregular*, with missing values and unevenly spaced measurements. These irregularities arise from limitations in data collection processes, such as sensor failures, inconsistent sampling, or interruptions in monitoring systems [24]. This irregularity poses a unique challenge for generating regular time series—where intervals are consistent, and the data follows the same distribution as if it were regularly observed [22]. The main goal of this paper is to generate regular sequences by training on irregularly-sampled time series using deep neural networks.

The synthesis of regular time series from irregular ones is a fundamental challenge, yet existing approaches remain scarce, with notable examples being GT-GAN and KoVAE [22, 35]. Unfortunately, these methods suffer from several limitations. First, they rely on generative adversarial networks (GANs) and variational autoencoders (VAEs), which have recently been surpassed in performance

*Equal Contribution

39th Conference on Neural Information Processing Systems (NeurIPS 2025).

by diffusion-based tools [8, 52, 34]. Second, both GT-GAN and KoVAE utilize a computationally-demanding preprocessing step based on neural controlled differential equations (NCDEs) [24], rendering these methods impractical for long time series. For instance, KoVAE requires $\approx 6.5\times$ more training time in comparison to our approach (See Fig. 3). Third, these methods inherently assume that the data, completed by NCDE, accurately reflects the true underlying distribution, which can introduce catastrophical errors when this assumption fails. In particular, their performance lags far behind that of models trained on regular time series, with state-of-the-art results on irregular discriminative benchmarks being, on average, 540% worse than those on regular benchmarks.

To address these shortcomings, we base our approach on a recent diffusion model for time series, ImagenTime [34]. This method maps time series data to images, enabling the use of powerful vision-based diffusion neural architectures. Leveraging a vision-based diffusion generator offers a significant advantage: regular time series can be generated from irregular ones using a straightforward masking mechanism. Specifically, missing values in the series are seamlessly ignored during the denoising process in training, akin to techniques used in image inpainting tasks [33, 9].

However, while this straightforward masking approach is simple and achieves strong results (see Tab. 8), we identify a significant limitation. Missing values in the time series are mapped to zeros in the image, resulting in "unnatural" neighborhoods that mix valid and invalid information. This can pose challenges for diffusion backbones, such as U-Nets with convolutional blocks, where the convolution kernels are not inherently masked and may inadvertently propagate errors from these artificial neighborhoods. To address this issue, we propose a two-step generation process. In the first step, we complete the irregular series using our adaptation of an efficient Time Series Transformer (TST) approach [54], significantly reducing computational overhead and enabling the generation of long time series. In the second step, we apply the straightforward masking approach described earlier. Crucially, this combination of completion and masking allows the model to learn from "natural" image neighborhoods while mitigating the reliance on fully accurate completed information through the use of masked loss minimization. Overall, our approach, built on a vision diffusion backbone, enables effective modeling of long time series while making minimal assumptions about pre-completed data, resulting in significantly efficient and improved generation performance.

We conduct a comprehensive evaluation of our approach on standard irregular time series benchmarks, benchmarking it against state-of-the-art methods. Our model consistently demonstrates superior generative performance, effectively bridging the gap between regular and irregular settings. Furthermore, we extend the evaluation to medium-, long- and ultra-long-length sequence generation, assessing performance across [12] datasets and 12 tasks. The results highlight the robustness and efficiency of our method, achieving consistent improvements over existing approaches. Our key contributions are summarized as follows:

1. We introduce a novel generative model for irregularly-sampled time series, leveraging vision-based diffusion approaches to efficiently and effectively handle sequences ranging from short to long lengths.
2. In contrast to existing methods that assume completed information is drawn from the data distribution, we treat it as a weak conditioning signal and directly optimize on the observed signal using a masking strategy.
3. Our approach achieves state-of-the-art performance across multiple generative tasks, delivering an average improvement of 70% in discriminative benchmarks while reducing computational requirements by 85% relative to competing methods.

2 Related Work

Diffusion models [43] have recently demonstrated groundbreaking generative capabilities, surpassing VAEs and GANs [25, 13] primarily on image generation [17, 11, 39]. The immense success of diffusion-based approaches has spurred a wave of recent advancements, encompassing both theoretical developments [44, 31] and practical applications [33, 18, 26].

Generative modeling of time series is an emerging field, with pioneering approaches predominantly relying on GANs [51, 29, 27] and VAEs [10, 35]. Recently, inspired by the success of diffusion models, there has been a growing trend to adapt these techniques to various time series tasks [46, 38], including generative modeling [8, 52]. Notably, the ImagenTime approach [34] has achieved state-of-the-art performance on regular generative tasks for sequences of varying lengths, from short to

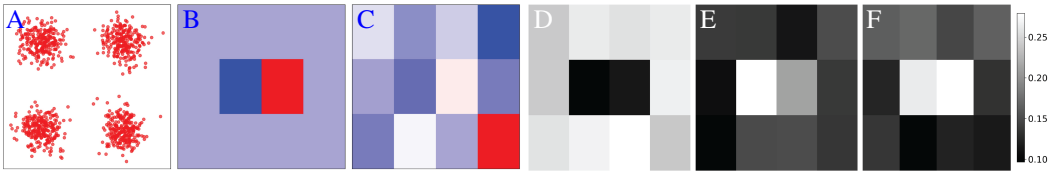

Figure 1: [TODO: Should be replaced by Nimrod together with the explanation] A data point (A) is mapped to an image with zeros and the coordinates in the center (B). Denoising the entire image yields inferior kernels (D) in comparison to masking (E). Constructing natural neighborhoods (C), yields consistent kernels and better scores (F).

very long, by transforming time series into images and leveraging vision-based diffusion backbones. Our work builds on ImagenTime, extending it to address the challenging setting of generating regular time series information from irregularly-sampled data.

Irregular time series modeling has been a longstanding task. Modern machine learning methods have made significant strides by framing the problem through the lens of differential equations [40, 24]. Subsequent efforts have explored alternative architectures, including recurrent neural networks [41] and transformers [54, 6]. However, learning from irregular sequences has received comparatively less attention, with notable contributions such as GT-GAN and KoVAE [22, 35], both relying on NCDE [24]. Despite their promise, NCDE-based methods are costly during preprocessing and training, limiting the applicability of GT-GAN and KoVAE in handling long time series. Further, replacing NCDE by efficient components such as TST [54], yields suboptimal results (see Tab. 8).

3 Background

Problem statement. We learn the underlying distribution of time series data from irregularly sampled observations and generating regular time series from it. Specifically, given a set of irregularly sampled sequences, our goal is to learn a model that approximates the true data distribution $p_{\text{data}}(x_{1:T})$ and enables sampling of complete time series $x_{1:T}$ from the learned distribution $p_\theta(x_{1:T})$. Formally, we consider a dataset of irregularly sampled time series, represented as $\{x^j_{t_1:t_n}\}_{j=1}^N$, where each sequence consists of observations at non-uniform time steps $t_1 : t_n = [t_1, t_2, \ldots, t_n]$ with $t_1 \geq 1$ and $t_n \leq T$. The challenge is to leverage these incomplete sequences to model the full distribution and generate realistic, regularly sampled time series that align with the true data distribution.

ImagenTime employs the delay embedding transformation to map time series data into images, enabling their processing with powerful vision-based diffusion models [34]. Given an input multivariate regular time series $x_{1:T} \in \mathbb{R}^{d \times T}$ with d features and length T, the delay embedding constructs an image $x_{\text{img}} \in \mathbb{R}^{d \times w \times h}$ by placing x's values over the columns of x_{img} per channel, where w, h are user-defined parameters. During training, noise is added to the image x_{img} at different timesteps, forming $x_{\text{img}}(t)$. The diffusion model, parameterized by s_θ, learns to denoise these images by approximating the score function $s_\theta(x_{\text{img}}, t)$. Inference begins with a noise sample $x_{\text{img}}(T) \sim \mathcal{N}(0, I)$. This sample is iteratively denoised using the learned score function to produce a cleaned image $x_{\text{img}}(0)$. The inverse delay embedding transform is then applied to $x_{\text{img}}(0)$, reconstructing the original time series $\tilde{x}_{1:T}$. Importantly, the inverse transformation of delay embedding is inherently non-unique, as the time series values are repeated within the image representation, suggesting various designs can be considered as we discuss in Sec. 4. Finally, a crucial advantage of ImagenTime is its effectivity in handling long series, e.g., a time series of length $65k$ is transformed to an image of size 256×256.

TST leverages the self-attention mechanism of Transformers to model temporal dependencies and long-range interactions in time-series data effectively. Unlike traditional sequence models such as RNNs or LSTMs, TST processes the entire sequence simultaneously, enabling parallelism and mitigating the vanishing gradient problem. The architecture includes input projection to a higher-dimensional feature space, positional encodings to capture temporal order, and a stack of Transformer encoder layers with flexible normalization and activation options. TST is particularly suitable for imputation tasks, as it can handle irregularly-sampled data and missing values through explicit masking and preprocessing. Additionally, its self-attention mechanism inherently supports long sequences, making it robust for capturing global context and dependencies in extended time-series data. By eliminating the need for computationally expensive preprocessing techniques, such as calculating coefficients for cubic splines or other interpolation methods, TST achieves significant

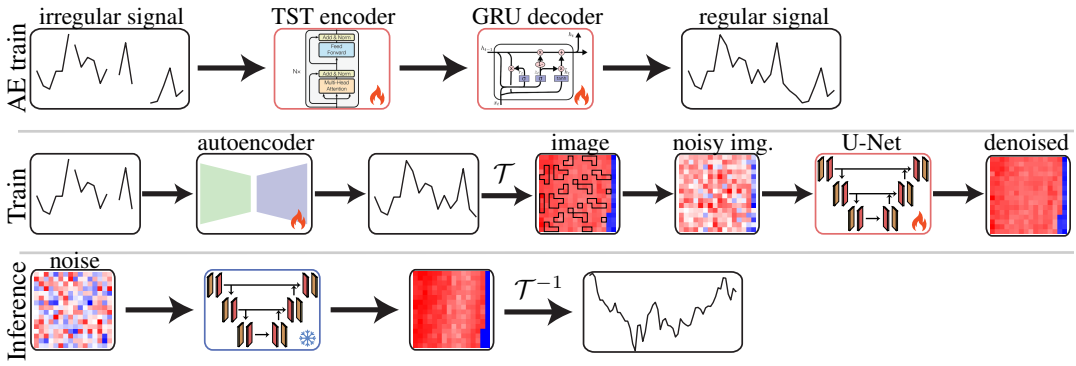

Figure 2: In the first step (top), we train a TST-based autoencoder, which we use during the second step (middle), where a vision diffusion model is trained with masking over non-active pixels. Inference (bottom) is done similarly to ImagenTime.

speed advantages while providing a scalable, efficient, and accurate solution for tasks like forecasting, classification, anomaly detection, and imputation.

4 Method

While ImagenTime does not address the challenge of irregularly-sampled time series, a simple extension can enable it to generate regularly-sampled time series by training on irregular data. The key idea involves employing a *mask* during the loss computation. This mask ensures that only "active" pixels–those corresponding to observed time series values–are considered in the loss calculation, while "non-active" pixels, representing missing information, are effectively ignored. This approach enables effective learning from incomplete data while preserving the integrity of the observed information, offering two key advantages: (i) the mask is architecture-agnostic, making it compatible with any diffusion backbone, and (ii) the inference procedure of ImagenTime remains entirely unchanged.

4.1 Unnatural image neighborhoods

Unfortunately, the straightforward approach has a fundamental limitation: although non-active pixels are ignored during loss computation, they are still processed by the network. In practice, missing values are replaced with zeros, resulting in "unnatural" pixel neighborhoods. Specifically, while zeros may occasionally occur in non-zero segments of a time series, their repeated presence is highly unlikely, leading to inconsistencies. In other words, masking is not applied at the architecture level, potentially hindering the effective learning of neural components.

To demonstrate this phenomenon, we consider the following toy experiment. We generate 1000 two-dimensional points, drawn from a multivariate Gaussian distribution with four centers (Fig. 1A). Given this distribution, we create an irregular dataset of 3×4 images, $\mathcal{S}_{\text{irregular}}$, by taking a data point, setting all pixels to zero except those at the center, corresponding to the x and y coordinates of the original point (Fig. 1B). Then, we train two diffusion models to: (i) predict the score across the entire image, and (ii) predict only the two central pixels via masking.

We evaluate the models by comparing their score estimation loss only on the two central pixels, regardless of the training strategy. Our results indicate that masking does *not* improve score estimation, yielding scores of 0.71 vs. 0.67 for Setups (i) and (ii), respectively. In addition, we also inspect the convolution kernels by averaging across channels the L_1 norm of each spatial position (Fig. 1D,E). As can be seen, the kernel in Setup (i) heavily attends to zero-valued pixels instead of focusing on the essential central pixels, suggesting that "unnatural" neighbors may be detrimental. In contrast, the masked kernel from Setup (ii) largely ignores non-relevant zeros and prioritizes the middle pixels.

4.2 Our approach

One possible solution to alleviate the phenomenon of unnatural neighborhoods is to implement masking at the kernel level, but this would require modifications tailored to each neural architecture, thereby restricting the approach's flexibility and its straightforward applicability across different models. For instance, while our work employs a convolutional U-Net, recent transformer-based architectures have emerged as highly effective diffusion backbones [36]. Accommodating such diversity in architectures would require a more generalized solution.

To create more natural pixel neighborhoods while remaining agnostic to the underlying architecture, we draw inspiration from the two-step process utilized in GT-GAN and KoVAE [22, 35]. Our approach adopts a two-step training scheme. First, we complete the missing values in the irregularly-sampled time series using TST [54], producing a regularly-sampled sequence. Next, we transform the completed time series into an image and apply denoising as in ImagenTime, with a key distinction: we apply the mask to the completed pixels during the loss computation (see App. B), as outlined in the straightforward approach discussed earlier. In the context of the toy experiment discussed in Sec. 4.1, the completed neighborhood (Fig. 1C) enables learning of consistent kernels (Fig. 1F), while improving score estimation (0.32).

This novel combination of completion and masking addresses the two primary challenges of processing irregular sequences. On one hand, it creates natural neighborhoods, enabling convolutional kernels to learn effectively from values that closely align with the true data distribution. On the other hand, it ensures that the completed values are not fully relied upon by excluding them from the loss computation via the mask, striking a balance between utilizing and mitigating incomplete information. An illustration of our approach is presented in Fig. 2, showing the autoencoder train (top), main train (middle), and inference (bottom) steps. $\mathcal{T}$ and $\mathcal{T}^{-1}$ represent the delay embedding transform and its inverse, and the fire and snowflake symbols refer to trainable and frozen modules.

Importantly, we identify limitations with $\mathcal{T}^{-1}$ that was proposed in [34]. Specifically, in their approach, only the first pixel corresponding to each time series value is used for reconstruction. Specifically, if x_i is mapped to multiple image indices, the original method selects the first corresponding pixel in the image for reconstruction. We modify this inverse transformation by aggregating information from all corresponding image indices and computing the average of the associated pixels for each x_i. For a given $x_{1:L} \in \mathbb{R}^L$, both methods ensure that $f^{-1}(f(x)) = x$. See Sec. 5.7 for an ablation study of these two methods.

5 Results

5.1 Quality vs. Complexity

In this experiment we compare the discriminative score and training time of our method against KoVAE across different sequence lengths $(24, 96, 768)$. Both models were evaluated under identical conditions, utilizing the same GPU and batch size to ensure a fair comparison. Training time was measured until each model converged to its best result. The discriminative score and training time were averaged over all missing rates and datasets for each sequence length and each method separately. As illustrated in Fig. 3 and Tab. 1, our approach achieves an average speedup of approximately **6.5**$\times$ and an average improvement of about **3.4**$\times$ in the discriminative score compared to KoVAE. The results demonstrate that our method not only trains significantly faster but also generates data that more closely resembles the real distribution compared to KoVAE. Full results can be seen in App. E.3

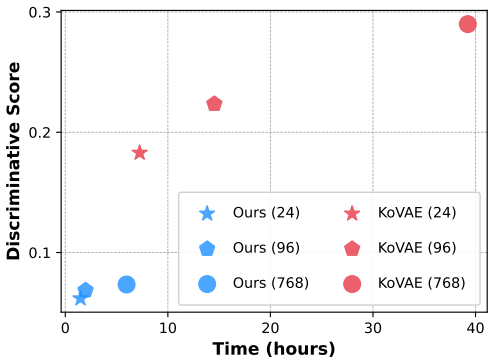

Figure 3: Comparison of discriminative score vs. training time for our approach and KoVAE across different sequence lengths $(24, 96,$ and $768)$. Lower discriminative scores and shorter training times are better.

Table 1: Training time (in hours) for sequence lengths (24, 96, and 768), averaged over 30%, 50%, and 70% missing rates.

	Model	ETTh1	ETTh2	ETTm1	ETTm2	Weather	Electricity	Energy	Sine	Stock	Mujoco
24	GT-GAN	7.44	3.68	5.14	3.60	5.04	6.45	5.25	4.09	3.15	2.17
	KoVAE	6.49	10.79	10.14	6.55	5.840	16.57	9.31	5.59	2.04	1.15
	Ours	**1.28**	**2.76**	**0.96**	**1.43**	**3.66**	**2.44**	**1.00**	**0.48**	**0.21**	**0.60**
96	KoVAE	19.70	10.82	14.61	26.51	22.06	-	13.68	10.76	6.45	-
	Ours	**1.52**	**1.90**	**1.24**	**1.85**	**1.87**	-	**1.72**	**1.46**	**0.76**	-
768	KoVAE	31.53	37.66	67.97	72.58	52.93	-	21.04	14.64	16.27	-
	Ours	**5.38**	**2.61**	**12.20**	**7.49**	**9.47**	-	**4.96**	**8.24**	**2.74**	-

Table 2: Averaged results over 30%, 50%, 70% missing rates for sequence length 24. Lower values are better.

	Model	ETTh1	ETTh2	ETTm1	ETTm2	Weather	Electricity	Energy	Sine	Stock
Disc.	TimeGAN-Δt	0.499	0.499	0.499	0.499	0.497	0.499	0.474	0.497	0.479
	GT-GAN	0.471	0.369	0.412	0.366	0.481	0.427	0.325	0.338	0.249
	KoVAE	0.197	0.081	0.050	0.067	0.332	0.498	0.323	0.043	0.118
	Ours	**0.037**	**0.009**	**0.012**	**0.011**	**0.057**	**0.384**	**0.080**	**0.010**	**0.008**
Pred.	TimeGAN-Δt	0.267	0.336	0.235	0.314	0.394	0.262	0.457	0.334	0.072
	GT-GAN	0.186	0.092	0.125	0.094	0.145	0.148	0.069	0.096	0.020
	KoVAE	0.057	0.054	0.045	0.050	0.057	**0.047**	0.050	0.074	0.017
	Ours	**0.053**	**0.046**	**0.044**	**0.044**	**0.022**	0.049	**0.047**	**0.069**	**0.012**
FID	TimeGAN-Δt	3.140	3.199	3.419	3.218	2.378	23.39	6.507	2.780	2.668
	GT-GAN	2.212	8.635	14.29	6.385	2.758	9.993	1.531	1.698	2.181
	KoVAE	1.518	0.248	0.180	0.280	3.699	6.163	0.629	0.037	0.369
	Ours	**0.124**	**0.035**	**0.047**	**0.024**	**0.170**	**3.580**	**0.132**	**0.015**	**0.036**
Corr.	TimeGAN-Δt	3.743	1.051	2.350	0.579	1.200	13.24	3.765	2.424	1.399
	GT-GAN	7.148	0.916	2.467	0.356	0.791	14.92	3.889	3.282	0.261
	KoVAE	0.183	0.177	0.130	0.262	2.899	4.283	2.630	0.041	0.064
	Ours	**0.084**	**0.054**	**0.065**	**0.039**	**0.396**	**2.031**	**0.922**	**0.015**	**0.019**

Table 3: Averaged results over 30%, 50%, 70% missing rates for sequence length 96 (top) and 768 (bottom).

		Model	ETTh1	ETTh2	ETTm1	ETTm2	Weather	Energy	Sine	Stock
Length $= 96$	**Disc.**	KoVAE	0.284	0.103	0.276	0.089	0.341	0.356	0.239	0.099
		Ours	**0.070**	**0.053**	**0.040**	**0.030**	**0.152**	**0.185**	**0.003**	**0.017**
	Pred.	KoVAE	0.062	0.057	0.054	0.050	0.046	0.080	0.165	0.020
		Ours	**0.053**	**0.049**	**0.045**	**0.044**	**0.025**	**0.049**	**0.155**	**0.011**
	FID	KoVAE	5.842	1.111	4.070	0.996	3.681	4.694	4.381	0.868
		Ours	**0.357**	**0.508**	**0.171**	**0.142**	**0.394**	**0.309**	**0.017**	**0.109**
	Corr.	KoVAE	0.224	0.362	0.175	0.435	2.609	4.810	0.222	0.089
		Ours	**0.114**	**0.151**	**0.092**	**0.094**	**0.890**	**1.161**	**0.016**	**0.014**
Length $= 768$	**Disc.**	KoVAE	0.238	0.201	0.236	0.196	0.428	0.384	0.350	0.284
		Ours	**0.088**	**0.045**	**0.058**	**0.052**	**0.102**	**0.213**	**0.006**	**0.022**
	Pred.	KoVAE	0.072	0.069	0.060	0.076	0.070	0.087	0.226	0.031
		Ours	**0.053**	**0.056**	**0.047**	**0.050**	**0.027**	**0.042**	**0.204**	**0.013**
	FID	KoVAE	13.92	8.304	13.50	8.279	17.49	24.51	38.60	7.273
		Ours	**0.882**	**0.439**	**0.391**	**0.264**	**0.318**	**0.796**	**0.237**	**0.160**
	Corr.	KoVAE	0.333	0.606	0.404	0.738	3.252	8.752	0.379	0.046
		Ours	**0.103**	**0.106**	**0.122**	**0.128**	**0.458**	**1.040**	**0.006**	**0.026**

5.2 Quantitative Evaluation.

Our quantitative evaluations assess missing rate setups of 30%, 50%, and 70%. For example, in the 30% missing rate case, we randomly omit 30% of the data in each training sample. Additionally, we extend the standard benchmark, which typically considers a sequence length of 24, to include longer sequences of 96, 768, and 10,920, providing a more comprehensive evaluation across varying temporal scales. We utilize a diverse set of datasets, extending beyond common benchmarks such as Sine, Stock, Energy, and MuJoCo to include additional real-world datasets: ETTh1, ETTh2, ETTm1, ETTm2, Weather, Electricity, KDD-Cup [and Traffic]. We compare against the popular TimeGAN approach [51], adapted to handle irregular data by incorporating the time difference between samples as input. In addition, we also consider the recent GT-GAN [22] and KoVAE [35].

We evaluate the performance of our model using the *discriminative* and *predictive* tasks suggested by [51]. In the discriminative task, we measure the similarity between real and synthetic samples by training a classifier to distinguish between the two, reporting $|0.5 - \text{acc}|$, where acc is the accuracy of the classifier. For the predictive task, we adopt the "train on synthetic, test on real" protocol, where a predictor is trained on synthetic data and tested on real data. The performance is evaluated using the Mean Absolute Error (MAE). We also consider irregular time series metrics: the *Context-FID score* [21], which quantifies the similarity in distribution between synthetic and real data, and the *correlation score* [29], which evaluates the feature-level relationship between the two datasets. The Context-FID score is computed by encoding both synthetic and real sequences using TS2Vec [53] and calculating the FID score on the representations. The correlation score measures the covariance of features between real and synthetic data, with a focus on assessing their alignment. Full details are provided in App. D.3. For all metrics, lower scores are better.

Tab. 2 details the benchmark results for a sequence length of 24. The values represent averages over the $30\%, 50\%$ and 70% missing rates, where the full results are provided in Tabs. 18. In general, our approach presents dramatic improvements across all metrics with respect to the second-best approach (typically KoVAE). Following [35], we define the relative improvement error as $e_{\text{rel}} = (e_2 - e_1)/e_2$, where e_2 is the second-best error and e_1 is ours. In this metric, averaged across all datasets, our method improves by **74.2%, 15.0%, 78.5%, 62.1%** in the discriminative, predictive, context-FID, and correlation scores, respectively. We also compared our approach to KoVAE in the medium (96) and long (768) lengths on all datasets excluding MuJoCo and electricity. The results appear in Tab. 3, showing the superiority of our method and its advantages to longer horizons, where we achieved mean relative improvement of $72.6\%, 29.7\%, 92.1\%$, and 73.25% in the discriminative, predictive, context-FID, and correlation scores. See the full results in Tabs. 19, 20. Finally, for ultra-long sequences (10,920) on the KDD-Cup dataset, our model showed improvements of **36.6%** in the discriminative score (see Tab. 4), showing its ability to generate realistic synthetic data even at extreme sequence lengths.

Table 4: Discriminative results of ultra-long (10,920) sequences on KDD-Cup for different missing rates.

Method	**30%**	**50%**	**70%**
KoVAE	0.375	0.410	0.499
Ours	**0.155**	**0.288**	**0.392**

5.3 Qualitative Evaluation

We evaluate the similarity between the generated sequences and the real data using qualitative metrics. Specifically, we employ two visualization techniques [51]: (i) projecting the real and synthetic data into a two-dimensional space using t-SNE [48], and (ii) performing kernel density estimation to visualize the corresponding probability density functions (PDFs). Fig. 4 illustrates these results for the 70% missing rate setting over various datasets and sequence lengths: Energy (24), Weather (96), and Stocks (768). The top row shows the two-dimensional point clouds of real (blue), KoVAE (green), and our data obtained via t-SNE, while the bottom row displays their respective PDFs. Overall, our approach demonstrates strong alignment in both visualizations. In the t-SNE plots (top row), a high degree of overlap between real and synthetic samples is observed. Similarly, in the PDF plots (bottom row), the trends and behaviors of the distributions are closely aligned. For additional results, including the regular and irregular 30% and 50% settings, please refer to App. E.2.

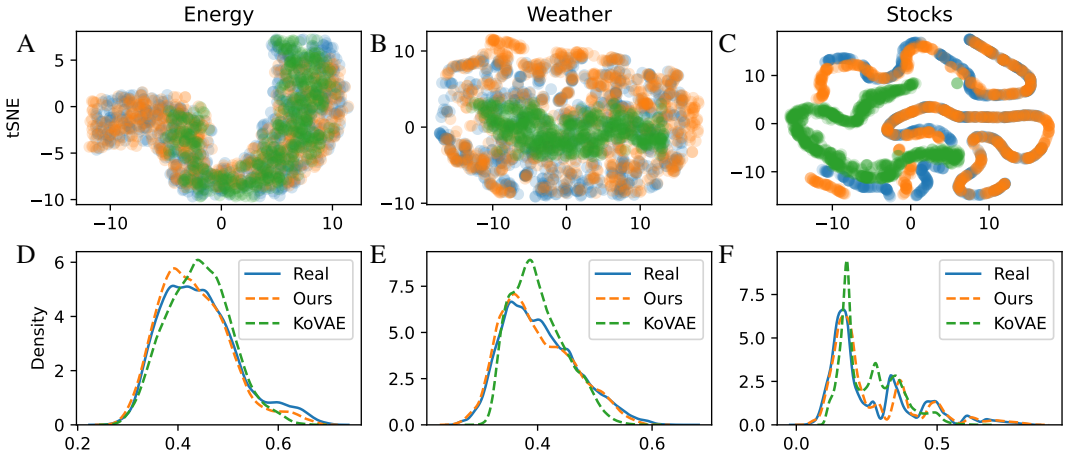

Figure 4: 2D t-SNE embeddings (top) and probability density functions (bottom) for real data vs. synthetic data from our method and KoVAE, under a 70% missing rate. From left to right: Energy (length 24), Weather (length 96), and Stock (length 768) datasets.

5.4 Irregularly-sampled data under noise

Our work primarily addresses irregularly sampled time series data. However, in real-world scenarios, such data often includes noise due to sensor limitations and inaccuracies. To further enhance our quantitative evaluation framework, we tackle the generative challenges of learning from irregular time series in noisy environments. Specifically, we propose a novel setup to evaluate the model's capability to recover the true underlying distribution from data corrupted by both irregular sampling and Gaussian noise. In this setup, we simulate a 50% missing rate and [inject additive Gaussian noise

Table 5: Discriminative and predictive scores for 50% missing rate on Weather, ETTh1, Stock, and Energy datasets with injected noise levels (0.1, 0.15, and 0.2).

N/R	Model	Weather		ETTh1		Stock		Energy	
		Disc.	Pred.	Disc.	Pred.	Disc.	Pred.	Disc.	Pred.
0.1	KoVAE	0.426	0.056	0.225	0.073	0.235	0.016	0.434	0.067
	Ours	**0.061**	**0.052**	**0.024**	**0.034**	**0.007**	**0.012**	**0.065**	**0.047**
0.15	KoVAE	0.488	0.092	**0.377**	0.077	0.341	0.092	0.493	0.093
	Ours	**0.416**	**0.029**	0.407	**0.059**	**0.282**	**0.023**	**0.467**	**0.053**
0.2	KoVAE	0.491	0.096	**0.440**	0.084	0.352	0.121	0.496	0.123
	Ours	**0.485**	**0.035**	0.456	**0.062**	**0.340**	**0.027**	**0.457**	**0.057**

Table 6: Discriminative and predictive scores for 40% random vs. 40% continuous missingness on the Weather and Energy datasets with sequence lengths of 24 and 96. Lower is better.

	Metric	Weather		Energy	
		Random	Continuous	Random	Continuous
Length = 24	Discriminative ↓	0.057	**0.053**	**0.081**	0.082
	Predictive ↓	**0.021**	0.025	0.047	**0.043**
Length = 96	Discriminative ↓	**0.154**	0.165	**0.185**	0.191
	Predictive ↓	0.025	**0.023**	**0.048**	0.050

sampled from a normal distribution $\mathcal{N}(0, \sigma)$, where σ corresponds to the specified noise level (e.g., $0.1, 0.15$, and 0.2). Importantly, this noise is added independently of the original data distribution or scale]. The evaluation is conducted on sequences of length 24 across four datasets: Weather, Etth1, Stocks. and Energy. Following the discriminative and predictive evaluation protocols for 50% missing rate described earlier, we compare our approach against the most recent state-of-the-art method, KoVAE. Tab. 5 presents the results. For each noise rate (N/R), we report the discriminative (Disc.) and predictive (Pred.) scores, where lower values indicate better performance. Our method consistently outperforms KoVAE, achieving significant improvements. Specifically, we observe an average relative improvement of **26.8%** in the discriminative score and **50.3%** in the predictive score across all datasets and noise levels.

5.5 Robustness to missingness patterns

[While many time series exhibit randomly missing values, in practice, missing values can also occur in contiguous blocks due to sensor outages or communication delays. To study this effect, we compare model performance under two types of 40% missingness: (i) randomly dropped values, and (ii) continuous missing blocks. This experiment is conducted on the Weather and Energy datasets using sequence lengths of 24 and 96. Discriminative and predictive scores are reported in Tab. 6. The results show that our method maintains strong performance under both missingness types, with some cases slightly favoring random missingness and others slightly favoring block-missingness. Overall, these findings confirm that our approach is robust across a range of missingness patterns, effectively handling both sporadic and structured data gaps.]

5.6 Extending to categorical and numerical features

[We further extend our evaluation to demonstrate that our method can handle mixed-type time series containing both numerical and categorical features. Categorical variables are mapped to learnable embedding vectors, which are jointly optimized with the generative model, transforming the input into a fully continuous representation that the diffusion process can operate on seamlessly. During generation, embeddings are mapped back to discrete categories using a simple postprocessing step. To validate this capability, we evaluated our method on the Traffic dataset which includes both numerical and categorical attributes, across multiple sequence lengths and missing rates. As reported in Tab. 7, our approach achieves the best discriminative scores compared to prior methods, demonstrating its ability to effectively capture temporal dependencies in mixed-type time series while maintaining superior generative performance.]

Table 7: [Discriminative scores of the ablation study with 30%, 50%, and 70% drop-rate on the Traffic dataset for sequence lengths of 24, and 96.]

	Model	30%	50%	70%
Len. = **24**	GT-GAN	0.481	0.473	0.485
	KoVAE	0.154	0.172	0.222
	Ours	**0.061**	**0.064**	**0.087**
Len. = **96**	GT-GAN	0.493	0.491	0.488
	KoVAE	0.212	0.245	0.307
	Ours	**0.073**	**0.091**	**0.102**

5.7 Ablation Studies

To better understand the contributions of each component in our proposed architecture, we conducted a series of ablation studies. We explore each of the components in our approach separately, and, additionally, we modify recent approaches to include our completion strategy. Specifically, we consider the following models: (i) KoVAE + TST, where the NCDE module in KoVAE is replaced by TST, as in our approach. (ii) TransFusion [42] + TST: Diffusion-based model designed for regular time series but not specifically for irregular time series data. Therefore, we used the TST module to impute the missing values. (iii) Mask Only, where the TST autoencoder is removed, and we only apply the masking mechanism. In this setup, missing values are imputed using unnatural neighbors by filling them with zeros. (iv) Ours Without Masking, where we leverage TST to complete missing values, and training is performed without masking. (v) Our approach.

We quantitatively evaluated each model under the same experimental conditions and show the results in Tab. 8. To provide an extensive analysis, our tests include several missing rates ($30\%, 50\%$, and 70%) using two datasets, Energy and Stock. Further, we measured the performance across different sequence lengths ($24, 96$, and 768). Our findings show that the combination of TST-based completion and masking yields superior performance compared to all other setups. Specifically, the Masking Only and Ours (Without Masking) setups showed significant limitations in capturing the true data distribution, while the replacement of NCDE with TST (KoVAE + TST) fell short in comparison to our proposed architecture. In particular, our results reveal that replacing the NCDE imputation component in KoVAE with the TST imputation mechanism is not the primary factor driving the significant improvements achieved by our method. Moreover, even when employing a powerful time series diffusion-based model like TransFusion combined with TST-based imputation, performance significantly degrades, struggling to capture the true distribution of the regular data. Overall, these results highlight the critical role of masking during the diffusion process and the importance of leveraging completion as a guide rather than a direct substitute for the true distribution.

We also ablate the impact of different image transformations on model performance, evaluating four methods: vanilla folding (reshapes a sequence into a fixed-size matrix with zero-padding), Gramian Angular Field, basic delay embedding, and our proposed inverse delay embedding (see App. A). Results in Tab. 9a and Tab. 12 show that geometric approaches—vanilla folding and our enhanced DE—better suit our method due to their structural clarity, where each pixel maps directly to a time point, facilitating mask usage and improving both discriminative and predictive performance. In contrast, GAF does not scale well to long sequences due to large image size. Our inverse transform also outperforms the original inverse of ImagenTime [34].

We also conducted an extensive ablation study comparing a variety of completion strategies. These included simple methods such as, Gaussian noise (GN), zero-filling, linear interpolation (LI), and polynomial interpolation (PI); probabilistic techniques like stochastic imputation (SI) (sampling from a Gaussian distribution fitted to the non-NaN values in each slice); and more advanced learning-based approaches, including NCDE, CSDI [46], and our proposed Time Series Transformer (TST) completion. Our results in Tab. 9b show that when the neighbors are not natural—such as in the case of zero completion or Gaussian noise completion—the model struggles more to generate data that closely follows the true distribution. In contrast, when using more natural completions (e.g., polynomial, stochastic imputation, NCDE, CSDI, TST), the model consistently obtains very good results. This confirms that generating natural neighborhoods indeed enhances the generative quality without making the model completely reliant on the imputation quality.

Table 8: Discriminative scores of the ablation study with 30%, 50%, and 70% drop-rate on Energy and Stock datasets for sequence lengths of 24, 96, and 768.

	Model	30%		50%		70%	
		Energy	Stock	Energy	Stock	Energy	Stock
Len. = 24	KoVAE + TST	0.399	0.109	0.407	0.064	0.408	0.037
	[TimeAutoDiff + TST]	0.293	0.100	0.329	0.101	0.468	0.375
	TransFusion + TST	0.201	0.050	0.279	0.058	0.423	0.065
	Ours (Mask Only)	0.157	0.087	0.269	0.168	0.372	0.237
	Ours (Without Mask)	0.158	0.025	0.307	0.045	0.444	0.013
	Ours	**0.048**	**0.007**	**0.065**	**0.007**	**0.128**	**0.007**
Len. = 96	KoVAE + TST	0.240	0.185	0.254	0.221	0.417	0.193
	[TimeAutoDiff + TST]	0.299	0.105	0.336	0.104	0.461	0.398
	TransFusion + TST	0.305	0.083	0.335	0.098	0.442	0.116
	Ours (Mask Only)	0.490	0.174	0.422	0.263	0.480	0.388
	Ours (Without Mask)	0.402	0.033	0.476	0.072	0.491	0.082
	Ours	**0.130**	**0.011**	**0.153**	**0.018**	**0.272**	**0.021**
Len. = 768	KoVAE + TST	0.380	0.225	0.418	0.243	0.385	0.186
	[TimeAutoDiff + TST]	0.299	0.104	0.334	0.101	0.466	0.487
	TransFusion + TST	0.367	0.113	0.395	0.121	0.451	0.131
	Ours (Mask Only)	0.437	0.249	0.349	0.450	0.435	0.491
	Ours (Without Mask)	0.364	0.027	0.353	0.102	0.325	0.102
	Ours	**0.170**	**0.025**	**0.244**	**0.033**	**0.251**	**0.013**

Table 9: Comparative performance on Energy and Stock datasets for sequence length 24.

(a) Ablation study on image transformation methods.

	Model	30%		50%		70%	
		Energy	Stock	Energy	Stock	Energy	Stock
Disc.	Gramian Angular	0.291	0.061	0.313	0.157	0.363	0.183
	Vanilla Folding	0.058	**0.005**	**0.050**	0.009	0.136	0.010
	Basic DE	0.091	0.035	0.102	0.046	0.153	0.019
	Ours DE	**0.048**	0.007	0.065	**0.007**	**0.128**	**0.007**
Pred.	Gramian Angular	0.049	0.013	0.048	0.015	0.049	0.016
	Vanilla Folding	0.047	0.013	0.047	0.013	0.047	0.014
	Basic DE	0.053	0.022	0.051	0.025	0.055	0.027
	Ours DE	**0.047**	**0.012**	**0.047**	**0.012**	**0.047**	**0.011**

(b) Imputation methods with 50% drop-rate.

Model	Disc.		Pred.	
	Energy	Stock	Energy	Stock
$GN \rightarrow$ NaN	0.457	0.102	0.058	0.014
$0 \rightarrow$ NaN	0.269	0.158	0.051	0.014
LI	0.251	0.013	0.049	0.019
PI	0.201	0.012	0.053	0.016
NCDE	0.102	0.013	0.058	0.013
CSDI	0.088	0.012	0.048	0.013
SI	0.069	0.010	0.047	0.013
[GRU-D]	0.158	0.014	0.055	0.015
Ours (TST)	**0.065**	**0.007**	**0.047**	**0.012**

[In addition to performance, we also compare the computational efficiency of completion strategies. Both NCDE and CSDI rely on costly operations—NCDE requires repeated cubic spline evaluations, while CSDI involves up to 1000 sampling steps per imputation—which makes them slow or infeasible for long sequences or high-dimensional data. In contrast, TST is lightweight and scales efficiently while still achieving competitive or superior results. As shown in Tab. 10, TST consistently trains faster and imputes orders of magnitude quicker than NCDE and CSDI; for instance, on the Energy dataset with sequence length 768, NCDE could not be trained due to memory limits and CSDI required over 84 hours of training and 2394 minutes for imputing 1024 samples, whereas TST completed training in just 6.67 hours and imputed all samples in only 6.26 seconds. These findings highlight TST's role as a scalable and efficient completion module, combining both high-quality generative performance and practical usability.]

[Finally, we investigate the impact of our integrated training scheme, which combines a short pre-training of the TST-based imputation module with joint training of both imputation and diffusion components. To assess its advantages, we compare three settings: (i) joint training with a brief TST pre-training (our approach), (ii) fully joint training from scratch, and (iii) a strict two-stage training where imputation is performed independently before generative training. Results in Tab. 11 demonstrate that our integrated approach consistently achieves the best discriminative performance across the Energy and Stock datasets, while fully joint training without pre-training suffers from unstable reconstructions, and the two-stage setup underperforms due to the lack of interaction between imputation and generative learning. These findings highlight that even a short pre-training phase can stabilize learning and enable the model to effectively leverage imputed values during generation.]

Table 10: [Training (200 epochs) and imputation (1024 samples) times on RTX 3090. TST is significantly faster than NCDE and CSDI, especially for long sequences; NCDE times are omitted where training was infeasible.]

Dataset	Seq. Len	TST (Ours)		NCDE		CSDI	
		Train (**h**)	Impute (**s**)	Train (**h**)	Impute (**s**)	Train (**h**)	Impute (**min**)
Energy	24	**0.67**	**0.64**	2.55	2.4	1.60	35.71
	96	**0.80**	**0.74**	7.68	5.6	5.43	135.29
	768	**6.67**	**6.26**	–	–	84.61	2394.71
Stock	24	**0.10**	**0.19**	0.67	2.0	0.18	15.40
	96	**0.13**	**0.20**	2.45	7.2	0.40	46.78
	768	**1.10**	**1.20**	59.32	56.0	3.55	514.08

Table 11: [Average discriminative scores across 30%, 50%, and 70% drop-rates on the Energy and Stock datasets for sequence length of 768.]

Model	Energy	Stock
Joint training without pre-training	0.278	0.076
Training independently	0.404	0.122
Joint training with pre-training (Ours)	**0.222**	**0.024**

6 Conclusions

In this work, we introduced a novel two-step framework for generating realistic regular time series from irregularly sampled sequences. By integrating a Time Series Transformer (TST) for completion with a vision-based diffusion model leveraging masking, we effectively addressed the challenge of unnatural neighborhoods inherent in direct masking approaches. This hybrid strategy ensures that the diffusion model benefits from more structured and meaningful input while mitigating over-reliance on completed values. Our extensive evaluations across multiple benchmarks demonstrated state-of-the-art performance, with improvements of up to 70% in discriminative score and an 85% reduction in computational cost over prior methods. Furthermore, our approach scales effectively to long time series, significantly outperforming existing generative models in both accuracy and efficiency.

Beyond these advancements, our work highlights the broader potential of integrating completion and masking strategies in generative modeling, particularly in domains where irregular sampling and missing values are prevalent. Future directions include extending our framework to multimodal time series generation, exploring self-supervised objectives for improved imputation, and integrating adaptive masking techniques that dynamically adjust completion reliance. By bridging the gap between irregular and regular time series generation, our method opens new possibilities for high-fidelity synthetic data generation in critical fields such as healthcare, finance, and climate science.

[

Acknowledgements

This research was partially supported by the Lynn and William Frankel Center of the Computer Science Department, Ben-Gurion University of the Negev, an ISF grant 668/21, an ISF equipment grant, and by the Israeli Council for Higher Education (CHE) via the Data Science Research Center, Ben-Gurion University of the Negev, Israel.]

References

[1] J. Allen. Short term spectral analysis, synthesis, and modification by discrete Fourier transform. *IEEE transactions on acoustics, speech, and signal processing*, 25(3):235–238, 1977.

[2] J. B. Allen and L. R. Rabiner. A unified approach to short-time Fourier analysis and synthesis. *Proceedings of the IEEE*, 65(11):1558–1564, 1977.

[3] E. Brophy, Z. Wang, Q. She, and T. Ward. Generative adversarial networks in time series: A systematic literature review. *ACM Computing Surveys*, 55(10):1–31, 2023.

[4] E. Brophy, Z. Wang, and T. E. Ward. Quick and easy time series generation with established image-based GANs. *arXiv preprint arXiv:1902.05624*, 2019.

[5] L. M. Candanedo, V. Feldheim, and D. Deramaix. Data driven prediction models of energy use of appliances in a low-energy house. *Energy and buildings*, 140:81–97, 2017.

[6] Y. Chen, K. Ren, Y. Wang, Y. Fang, W. Sun, and D. Li. ContiFormer: Continuous-time transformer for irregular time series modeling. *Advances in Neural Information Processing Systems*, 37, 2023.

[7] Z. Chen, Y. Wu, Y. Leng, J. Chen, H. Liu, X. Tan, Y. Cui, K. Wang, L. He, S. Zhao, J. Bian, and D. P. Mandic. ResGrad: Residual denoising diffusion probabilistic models for text to speech. *arXiv preprint arXiv:2212.14518*, 2022.

[8] A. Coletta, S. Gopalakrishnan, D. Borrajo, and S. Vyetrenko. On the constrained time-series generation problem. *Advances in Neural Information Processing Systems*, 37, 2023.

[9] C. Corneanu, R. Gadde, and A. M. Martinez. LatentPaint: Image inpainting in latent space with diffusion models. In *Proceedings of the IEEE/CVF Winter Conference on Applications of Computer Vision*, pages 4334–4343, 2024.

[10] A. Desai, C. Freeman, Z. Wang, and I. Beaver. TimeVAE: A variational auto-encoder for multivariate time series generation. *arXiv preprint arXiv:2111.08095*, 2021.

[11] P. Dhariwal and A. Nichol. Diffusion models beat GANs on image synthesis. *Advances in neural information processing systems*, 34:8780–8794, 2021.

[12] P. Flandrin, G. Rilling, and P. Goncalves. Empirical mode decomposition as a filter bank. *IEEE signal processing letters*, 11(2):112–114, 2004.

[13] I. J. Goodfellow, J. Pouget-Abadie, M. Mirza, B. Xu, D. Warde-Farley, S. Ozair, A. C. Courville, and Y. Bengio. Generative adversarial nets. In *Advances in Neural Information Processing Systems 27*, pages 2672–2680, 2014.

[14] Z. Han, J. Zhao, H. Leung, K. F. Ma, and W. Wang. A review of deep learning models for time series prediction. *IEEE Sensors Journal*, 21(6):7833–7848, 2019.

[15] N. Hatami, Y. Gavet, and J. Debayle. Classification of time-series images using deep convolutional neural networks. In *Tenth international conference on machine vision (ICMV 2017)*, volume 10696, pages 242–249. SPIE, 2018.

[16] J. Hellermann and S. Lessmann. Leveraging image-based generative adversarial networks for time series generation. *arXiv preprint arXiv:2112.08060*, 2021.

[17] J. Ho, A. Jain, and P. Abbeel. Denoising diffusion probabilistic models. *Advances in neural information processing systems*, 33:6840–6851, 2020.

[18] J. Ho, T. Salimans, A. Gritsenko, W. Chan, M. Norouzi, and D. J. Fleet. Video diffusion models. *Advances in Neural Information Processing Systems*, 35:8633–8646, 2022.

[19] J. Hogue. Metro Interstate Traffic Volume. UCI Machine Learning Repository, 2019. DOI: https://doi.org/10.24432/C5X60B.

[20] H. Ismail Fawaz, G. Forestier, J. Weber, L. Idoumghar, and P.-A. Muller. Deep learning for time series classification: a review. *Data mining and knowledge discovery*, 33(4):917–963, 2019.

[21] P. Jeha, M. Bohlke-Schneider, P. Mercado, S. Kapoor, R. S. Nirwan, V. Flunkert, J. Gasthaus, and T. Januschowski. PSA-GAN: Progressive self attention GANs for synthetic time series. In *The Tenth International Conference on Learning Representations*, 2022.

[22] J. Jeon, J. Kim, H. Song, S. Cho, and N. Park. GT-GAN: General purpose time series synthesis with generative adversarial networks. *Advances in Neural Information Processing Systems*, 35:36999–37010, 2022.

[23] T. Karras, M. Aittala, T. Aila, and S. Laine. Elucidating the design space of diffusion-based generative models. *Advances in neural information processing systems*, 35:26565–26577, 2022.

[24] P. Kidger, J. Morrill, J. Foster, and T. Lyons. Neural controlled differential equations for irregular time series. *Advances in Neural Information Processing Systems*, 33:6696–6707, 2020.

[25] D. P. Kingma and M. Welling. Auto-encoding variational Bayes. In *2nd International Conference on Learning Representations, ICLR*, 2014.

[26] F. Kreuk, G. Synnaeve, A. Polyak, U. Singer, A. Défossez, J. Copet, D. Parikh, Y. Taigman, and Y. Adi. AudioGen: Textually guided audio generation. In *The Eleventh International Conference on Learning Representations, ICLR*, 2023.

[27] X. Li, V. Metsis, H. Wang, and A. H. H. Ngu. TTS-GAN: A transformer-based time-series generative adversarial network. In *International conference on artificial intelligence in medicine*, pages 133–143. Springer, 2022.

[28] Z. Li, S. Li, and X. Yan. Time series as images: Vision transformer for irregularly sampled time series. *Advances in Neural Information Processing Systems*, 36, 2023.

[29] S. Liao, H. Ni, L. Szpruch, M. Wiese, M. Sabate-Vidales, and B. Xiao. Conditional Sig-Wasserstein GANs for time series generation. *arXiv preprint arXiv:2006.05421*, 2020.

[30] B. Lim and S. Zohren. Time-series forecasting with deep learning: a survey. *Philosophical Transactions of the Royal Society A*, 379(2194):20200209, 2021.

[31] Y. Lipman, R. T. Q. Chen, H. Ben-Hamu, M. Nickel, and M. Le. Flow matching for generative modeling. In *The Eleventh International Conference on Learning Representations, ICLR*, 2023.

[32] H. Liu, Z. Chen, Y. Yuan, X. Mei, X. Liu, D. Mandic, W. Wang, and M. D. Plumbley. AudioLDM: Text-to-audio generation with latent diffusion models. In *Proceedings of the 40th International Conference on Machine Learning*, volume 202 of *Proceedings of Machine Learning Research*, pages 21450–21474. PMLR, 23–29 Jul 2023.

[33] A. Lugmayr, M. Danelljan, A. Romero, F. Yu, R. Timofte, and L. Van Gool. Repaint: Inpainting using denoising diffusion probabilistic models. In *Proceedings of the IEEE/CVF conference on computer vision and pattern recognition*, pages 11461–11471, 2022.

[34] I. Naiman, N. Berman, I. Pemper, I. Arbiv, G. Fadlon, and O. Azencot. Utilizing image transforms and diffusion models for generative modeling of short and long time series. *Advances in Neural Information Processing Systems*, 38, 2024.

[35] I. Naiman, N. B. Erichson, P. Ren, M. W. Mahoney, and O. Azencot. Generative modeling of regular and irregular time series data via Koopman VAEs. In *The Twelfth International Conference on Learning Representations, ICLR*, 2024.

[36] W. Peebles and S. Xie. Scalable diffusion models with transformers. In *Proceedings of the IEEE/CVF International Conference on Computer Vision*, pages 4195–4205, 2023.

[37] V. Popov, I. Vovk, V. Gogoryan, T. Sadekova, and M. Kudinov. Grad-TTS: A diffusion probabilistic model for text-to-speech. In *International Conference on Machine Learning*, pages 8599–8608. PMLR, 2021.

[38] K. Rasul, C. Seward, I. Schuster, and R. Vollgraf. Autoregressive denoising diffusion models for multivariate probabilistic time series forecasting. In *International Conference on Machine Learning*, pages 8857–8868. PMLR, 2021.

[39] R. Rombach, A. Blattmann, D. Lorenz, P. Esser, and B. Ommer. High-resolution image synthesis with latent diffusion models. In *Proceedings of the IEEE/CVF conference on computer vision and pattern recognition*, pages 10684–10695, 2022.

[40] Y. Rubanova, R. T. Chen, and D. K. Duvenaud. Latent ordinary differential equations for irregularly-sampled time series. *Advances in neural information processing systems*, 32, 2019.

[41] M. Schirmer, M. Eltayeb, S. Lessmann, and M. Rudolph. Modeling irregular time series with continuous recurrent units. In *International conference on machine learning*, pages 19388–19405. PMLR, 2022.

[42] M. F. Sikder, R. Ramachandranpillai, and F. Heintz. Transfusion: Generating long, high fidelity time series using diffusion models with transformers. *arXiv preprint arXiv:2307.12667*, 2023.

[43] J. Sohl-Dickstein, E. Weiss, N. Maheswaranathan, and S. Ganguli. Deep unsupervised learning using nonequilibrium thermodynamics. In *International conference on machine learning*, pages 2256–2265. PMLR, 2015.

[44] Y. Song, J. Sohl-Dickstein, D. P. Kingma, A. Kumar, S. Ermon, and B. Poole. Score-based generative modeling through stochastic differential equations. In *9th International Conference on Learning Representations, ICLR*, 2021.

[45] F. Takens. Detecting strange attractors in turbulence. In *Dynamical Systems and Turbulence, Warwick 1980: proceedings of a symposium held at the University of Warwick 1979/80*, pages 366–381. Springer, 2006.

[46] Y. Tashiro, J. Song, Y. Song, and S. Ermon. CSDI: Conditional score-based diffusion models for probabilistic time series imputation. *Advances in Neural Information Processing Systems*, 34:24804–24816, 2021.

[47] E. Todorov, T. Erez, and Y. Tassa. MuJoCo: A physics engine for model-based control. In *2012 IEEE/RSJ international conference on intelligent robots and systems*, pages 5026–5033. IEEE, 2012.

[48] L. Van der Maaten and G. Hinton. Visualizing data using t-SNE. *Journal of machine learning research*, 9(11), 2008.

[49] M. Vetterli and C. Herley. Wavelets and filter banks: Theory and design. *IEEE transactions on signal processing*, 40(9):2207–2232, 1992.

[50] Z. Wang and T. Oates. Imaging time-series to improve classification and imputation. In *Proceedings of the Twenty-Fourth International Joint Conference on Artificial Intelligence, IJCAI*, pages 3939–3945. AAAI Press, 2015.

[51] J. Yoon, D. Jarrett, and M. Van der Schaar. Time-series generative adversarial networks. *Advances in neural information processing systems*, 32, 2019.

[52] X. Yuan and Y. Qiao. Diffusion-TS: Interpretable diffusion for general time series generation. In *The Twelfth International Conference on Learning Representations, ICLR*, 2024.

[53] Z. Yue, Y. Wang, J. Duan, T. Yang, C. Huang, Y. Tong, and B. Xu. TS2Vec: Towards universal representation of time series. In *Proceedings of the AAAI Conference on Artificial Intelligence*, volume 36, pages 8980–8987, 2022.

[54] G. Zerveas, S. Jayaraman, D. Patel, A. Bhamidipaty, and C. Eickhoff. A transformer-based framework for multivariate time series representation learning. In *Proceedings of the 27th ACM SIGKDD conference on knowledge discovery & data mining*, pages 2114–2124, 2021.

[55] H. Zhou, S. Zhang, J. Peng, S. Zhang, J. Li, H. Xiong, and W. Zhang. Informer: Beyond efficient transformer for long sequence time-series forecasting. In *Proceedings of the AAAI conference on artificial intelligence*, volume 35, pages 11106–11115, 2021.

A Time Series-to-Image Transformation

In this section, we provide a brief discussion on time series to image conversions. We then introduce Delay Embedding, the transformation we employed. Additionally, we describe an improvement we implemented to enhance the reversibility of delay embedding.

Time series to image conversion. The conversion of time series data into image representations has attracted significant interest for its ability to leverage computer vision methods in time series analysis. Techniques like Gramian Angular Fields [50], Recurrence Plots [15], and Line Graphs [28] allow for mapping time series data to visual formats, enabling tasks such as classification and imputation. In the field of speech analysis, the short-time Fourier transform (STFT) [1, 2, 49, 12] is crucial for capturing frequency variations over time, which is vital for processing audio and speech data. Recent advancements have also explored incorporating mel-spectrograms in diffusion models, particularly in connection with latent diffusion spaces[37, 7, 32]. Furthermore, generative approaches such as Wasserstein GANs [4, 16] have been applied to time series in image form.

Vanilla Folding is a straightforward transformation. Given a time series x, we reshape it into an image x_{img} by filling rows from left to right and moving to the next row upon reaching the end, padding with zeros if necessary. The inverse transformation reconstructs the original time series by reading the non-padded region row-wise. Despite its simplicity, this method scales well to very long sequences. Folding can also be interpreted as a specific case of delay embedding, as we explain below.

Delay Embedding and Enhanced Reverse Transformation [45] converts a univariate time series $x_{1:L} \in \mathbb{R}^L$ into an image by structuring its information into columns and applying zero-padding as needed. This transformation is controlled by two hyperparameters: m, which defines the skip value, and n, which determines the number of columns. Given any channel of a time series, the corresponding matrix X is formed as follows:

$$X = \begin{bmatrix} x_1 & x_{m+1} & \dots & x_{L-n} \\ \vdots & \vdots & \dots & \vdots \\ x_n & x_{n+m+1} & \dots & x_L \end{bmatrix} \in \mathbb{R}^{n \times q},$$

where $q = \lceil (L-n)/m \rceil$. To match the input requirements of a neural network, the resulting image x_{img} is padded with zeros. This transformation is applied independently to each channel, and for multivariate time series, the matrices X from different channels are concatenated along a new axis. Given an input signal $x \in \mathbb{R}^{L \times K}$, the output is a transformed representation $x_{\text{img}} \in \mathbb{R}^{K \times n \times q}$, which is then zero-padded to obtain $x_{\text{img}} \in \mathbb{R}^{K \times n \times n}$. Delay embedding efficiently scales to long sequences; for instance, choosing $m = n = 256$ enables the encoding of sequences up to $65k$ in length using 256×256 images.

Our primary innovation lies in the reverse transformation process. In the original approach, only the first pixel corresponding to each time series value is used for reconstruction. Specifically, if x_i is mapped to multiple image indices, the original method selects the first corresponding pixel in the image for reconstruction. In contrast, our approach aggregates information from all corresponding image indices by computing the average of the associated pixels for each x_i. For a given $x_{1:L} \in \mathbb{R}^L$, both methods ensure that $f^{-1}(f(x)) = x$.

As shown in Table 12, our approach consistently outperforms the original approach across various drop rates. For example, at a 30% drop rate, our delay embedding (DE) approach achieves a discriminative score of 0.020 for the ETTh1 dataset and 0.009 for ETTh2, compared to 0.023 and 0.018 with the naive approach, respectively. Similarly, at a 50% drop rate, the new DE method reduces the discriminative score to 0.032 (ETTh1) and 0.005 (ETTh2), outperforming the previous DE approach, which yielded scores of 0.040 and 0.037, respectively.

Table 12: Discriminative scores on ETTh1 and ETTh2 for sequence length 24 to compare the original inverse delay embedding vs. our inverse, evaluated in $30\%, 50\%$, and 70% missing rates.

Model	30%		50%		70%	
	ETTh1	ETTh2	ETTh2	ETTh2	ETTh2	ETTh2
Ours + Old inverse	0.023	0.018	0.040	0.037	0.067	0.048
Ours + New inverse	**0.020**	**0.009**	**0.032**	**0.005**	**0.058**	**0.013**

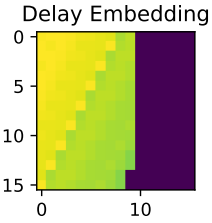

B Training Losses

Our model consists of two main components: an Autoencoder (AE) and a vision diffusion model (ImagenTime). For each component, we modified the loss to handle irregular data more effectively.

B.1 Autoencoder Training Loss

The TST-Based AE is trained to reconstruct only the known (non-missing) values of the input data. Since we do not have access to the regularly sampled time series during training, the model learns to infer missing values from the irregularly sampled data. The masked reconstruction loss is defined as:

$$\mathcal{L}_e^{t=0} = \frac{1}{|\mathcal{O}|} \sum_{i \in \mathcal{O}} (\tilde{x}_i - x_i)^2 \tag{1}$$

where x is the original input data, $\tilde{x}$ is the reconstructed output, $\mathcal{O}$ represents the set of observed (non-missing) indices in the input x, and $|\mathcal{O}|$ is the number of observed values. This ensures that the loss function only penalizes reconstruction errors for the known values, without considering the missing ones.

B.2 ImagenTime Diffusion Training Loss

At the core of **ImagenTime** is the generative diffusion model, which follows the framework of Karras et al. [23] for improved score-based modeling. The model employs a second-order ODE for the reverse process, balancing fast sampling and high-quality generations.

For irregular time series data, we changed the training loss to ensure proper weighting of the diffusion steps and account for missing values. Given an input sequence x and a corresponding mask m indicating observed entries, the loss is defined as:

$$\mathcal{L}_{\text{diff}} = \mathbb{E}_{x,\sigma} \left[\| (D_\theta(x + \sigma n, \sigma) - x) \cdot m \|^2 \right] \tag{2}$$

where:

- x is the input time series with missing values.
- $n \sim \mathcal{N}(0, I)$ is standard Gaussian noise, scaled by σ.
- m is the mask, indicating the observed values.

The model reconstructs the output using both observed and imputed indices, treating the imputed values as natural neighbors to the observed ones. However, the loss is computed and compared only against the observed indices, ensuring that the comparison is made solely to the true distribution, unaffected by the imputed values. This allows the model to learn the distribution while maintaining accurate reconstruction of missing values.

C Inference Time Analysis

In this section, we present a detailed comparison of the inference time between our approach and KoVAE, particularly in relation to sequence length. The evaluation is conducted across a range of sequence lengths: 24, 96, and 768. Additionally, we explore the relationship between inference time and sequence length for both models.

C.1 Inference Time vs. Sequence Length

Figure 5 illustrates the relationship between inference time per sample (in seconds) and sequence length for both our model and KoVAE. While KoVAE demonstrates faster sampling on short sequences, its efficiency degrades rapidly as the sequence length increases. KoVAE, which is based on a sequential VAE architecture for time series, processes each time step individually throughout the entire sequence, causing its computational cost to increase significantly with longer sequences and resulting in substantially longer inference times.

In contrast, our model maintains nearly constant inference time regardless of sequence length, making it highly efficient even for sequences as long as 5000 time steps. This is due to the use of delay embedding, which enables the model to compress long sequences into compact image representations with fixed dimensions. A clear turning point occurs at a sequence length of approximately 4500, beyond which our model consistently outperforms KoVAE in terms of inference time. This robust performance highlights the advantage of our method in terms of time efficiency, especially when dealing with long sequences.

C.2 Inference Time and Fidelity Comparison

As shown in Figure 6, we evaluate the relationship between inference time and fidelity (indicated by the discriminative score) for a single sequence. Lower discriminative scores correspond to higher fidelity in the model's predictions. On the other hand, inference time is a measure of efficiency, with shorter times indicating greater computational efficiency.

Our approach consistently performs well by maintaining a low discriminative score, which translates into higher fidelity in its predictions. This is achieved while also managing to keep the inference time relatively low, even for longer sequences. Notably, our model uses only 18 sampling steps regardless of sequence length, which results in stable and fast inference times across all configurations.

C.3 Performance Comparison

As observed from both figures, our model exhibits a favorable trade-off between inference efficiency and fidelity. While KoVAE might be more efficient for shorter sequences, its performance degrades as sequence length increases, making it less suitable for long sequences. Our approach, however, remains consistently efficient and accurate, maintaining both low discriminative scores and linear inference times as sequence lengths scale.

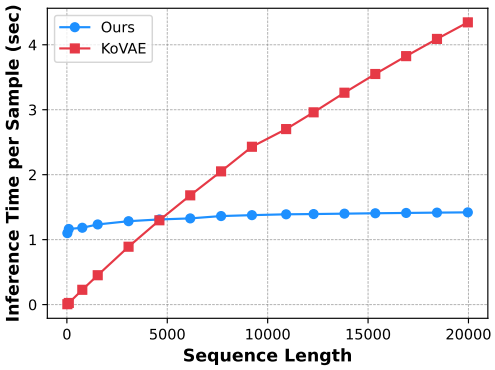

Figure 5: Comparison of inference time per sample in seconds vs. sequence length of our model and KoVae model.

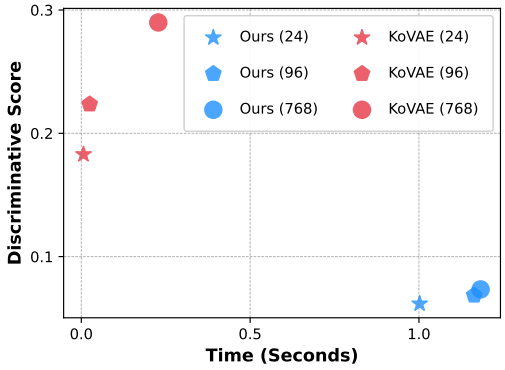

Figure 6: Comparison of discriminative score vs. inference time of a single sequence for our approach and KoVAE across different sequence lengths $(24, 96, \text{and } 768)$. Lower discriminative scores indicate higher fidelity, and shorter inference times reflect greater efficiency.

D Experimental Setup

D.1 Baseline Methods

We compare our method with several generative time series models designed for irregular data. KoVAE [35] is specifically designed to handle irregularly sampled time series effectively. Additionally, we consider GT-GAN [22], another method tailored for irregular time series generation. Lastly, we evaluate against TimeGAN-Δt [51], a re-designed version of the original TimeGAN. Since TimeGAN does not natively support irregular time series, we follow GT-GAN and compare them with their re-designed versions. Specifically, extending regular approaches to support irregular TS requires the conversion of a dynamical module to its time-continuous version. we adapted it by converting its GRU layers to GRU-Δt, enabling the model to exploit the time differences between observations and capture temporal dynamics.

D.2 Datasets

We conduct experiments using a combination of synthetic and real-world datasets, each designed to evaluate the model under various conditions, including regular and irregular time-series settings.

Sines This synthetic dataset contains 5 features, where each feature is independently generated using sinusoidal functions with different frequencies and phases. Specifically, for each feature $i \in \{1, ..., 5\}$, the time-series data is defined as $x_i(t) = \sin(2\pi f_i t + \theta_i)$, where $f_i \sim U[0, 1]$ and $\theta_i \sim U[-\pi, \pi]$. The dataset is characterized by its continuity and periodic properties, making it a suitable benchmark for evaluating the model's ability to handle structured time-series data.

Stocks The Stocks dataset comprises daily historical Google stock price data from 2004 to 2019. It includes six features: high, low, opening, closing, adjusted closing prices, and trading volume. Unlike Sines, this dataset lacks periodicity and primarily exhibits random walk patterns. It is a real-world dataset commonly used to benchmark financial time-series forecasting and modeling.

MuJoCo MuJoCo (Multi-Joint dynamics with Contact) is a versatile physics simulation framework used to generate multivariate time-series data [47]. The dataset contains 14 features representing state variables and control actions from simulated trajectories. This dataset is particularly suitable for evaluating models on dynamical systems and tasks involving physical interactions

Energy The Energy dataset is a real-world multivariate time-series dataset [5] derived from the UCI Appliance Energy Prediction dataset. It includes 28 features, which are correlated and exhibit noisy periodicity and continuous-valued measurements. This dataset provides a challenging benchmark for forecasting and modeling tasks involving environmental and appliance energy consumption data.

ETTh & ETTm The ETTh (Electricity Transformer Temperature - Hourly) and ETTm (Electricity Transformer Temperature - Minute) datasets [55] capture electricity load data from two power stations with varying temporal resolutions. These datasets are used for short- and long-term time-series forecasting tasks and are part of an established benchmark for evaluating generative and predictive models.

Weather The Weather dataset includes daily meteorological measurements, such as temperature, precipitation, snowfall, snow depth, and minimum and maximum temperatures, collected from the United States Historical Climatology Network (USHCN) [2] . The dataset comprises measurements from 1,218 weather stations and is used for analyzing climatic trends and weather forecasting tasks.

Electricity The Electricity dataset consists of electricity consumption data across multiple clients, represented as multivariate time-series. It is widely used for forecasting electricity loads and understanding temporal consumption patterns in energy-related applications.

[2] `https://knb.ecoinformatics.org/view/doi%3A10.3334%2FCDIAC%2FCLI.NDP019`

Traffic [The Traffic dataset [19] contains hourly traffic volume data for westbound I-94 in the Minneapolis-St. Paul, MN area, collected from 2012 to 2018. It includes eight features, mixing numerical measurements (e.g., temperature, rainfall, snowfall, cloud coverage, traffic volume) with several categorical variables (e.g., holiday indicators, weather descriptions), making it one of the few benchmarks that requires models to handle both continuous and categorical time-series data. The dataset captures multivariate, sequential patterns influenced by weather and holiday effects, making it particularly suitable as a generative benchmark for modeling complex dependencies across heterogeneous features.]

D.3 Metrics

Discriminative Score This metric measures the ability of a model to differentiate between real and generated data. A lower discriminative score indicates that the generated data is more indistinguishable from the real data, reflecting better generative performance. This score is typically computed by training a binary classifier and evaluating its accuracy in distinguishing between the two datasets. A score close to random guessing suggests that the synthetic data is nearly indistinguishable from real data.

Predictive Score The predictive score evaluates the quality of the generated data in terms of its utility for downstream predictive tasks. It is typically assessed using a supervised learning model trained on generated data and tested on real data, or vice versa. A higher predictive score indicates better alignment between real and generated distributions.

Context-FID Score A lower Frechet Inception Distance (FID) score indicates that synthetic sequences are more similar to the original data distribution. Paul et al. (2022) introduced a variation of FID, called Context-FID (Context-Frechet Inception Distance), which replaces the Inception model in the original FID calculation with TS2Vec, a time series representation learning method [53]. Their findings suggest that models with the lowest Context-FID scores tend to achieve the best results in downstream tasks. Additionally, they demonstrated a strong correlation between the Context-FID score and the forecasting performance of generative models. To compute this score, synthetic and real time series samples are first generated, then encoded using a pre-trained TS2Vec model, after which the FID score is calculated based on the learned representations.

Correlational Score Building on the approach from [29], we estimate the covariance between the i^{th} and j^{th} features of a time series using the following formula:

$$\text{cov}_{i,j} = \frac{1}{T}\sum_{t=1}^{T} X_t^i X_t^j - \left(\frac{1}{T}\sum_{t=1}^{T} X_t^i\right)\left(\frac{1}{T}\sum_{t=1}^{T} X_t^j\right).$$

To quantify the correlation between real and synthetic data, we compute the following metric:

$$\frac{1}{10}\sum_{i,j}\left|\frac{\text{cov}_r^{i,j}}{\sqrt{\text{cov}_r^{i,i}\,\text{cov}_r^{j,j}}} - \frac{\text{cov}_f^{i,j}}{\sqrt{\text{cov}_f^{i,i}\,\text{cov}_f^{j,j}}}\right|$$

D.4 Hyperparameters.

We summarize the key hyperparameters used in our framework in Tables 13, 14, and 15, corresponding to sequence lengths of 24, 96, and 768, respectively. The hyperparameters remain largely consistent across tasks, with variations in batch size, embedding dimensions, and image resolutions. We use the default EDM [23] sampler for all datasets and follow a unified configuration for the U-Net architecture in the diffusion model. For further details, refer to [23]. Additionally, all models were trained using the same learning rate schedule and optimization settings to ensure comparability across different sequence lengths.

Table 13: Hyperparameter Settings for Sequence Length 24 Across Different Datasets

	ETTh1	ETTh2	ETTm1	ETTm2	Weather	Electricity	Energy	Sine	Stock	Mujoco
General										
image size	16×16	16×16	16×16	16×8	8×8	8×8	8×8	8×8	8×8	8×8
learning rate	10^{-4}	10^{-4}	10^{-4}	10^{-4}	10^{-4}	10^{-4}	10^{-4}	10^{-4}	10^{-4}	10^{-4}
batch size	128	128	128	128	128	128	128	128	128	128
teacher forcing rate	0	0	0	0	0	0	0	0	0.2	0
DE										
embedding(n)	8	8	8	8	8	8	8	8	8	8
delay(m)	3	3	3	3	3	3	3	3	3	3
TST										
hidden_dim	40	40	40	40	40	40	40	40	40	40
n_heads	5	5	5	5	5	5	5	5	5	5
num_layers	6	6	6	6	6	6	6	6	6	6
Diffusion										
U-net channels	128	128	128	128	128	128	128	128	128	64
in channels	$[1, 2, 2, 2]$	$[1, 2, 2, 2]$	$[1, 2, 2, 2]$	$[1, 2, 2, 2]$	$[1, 2, 2, 4]$	$[1, 2, 2, 4]$	$[1, 2, 2, 4]$	$[1, 2, 2, 2]$	$[1, 2, 2, 2]$	$[1, 2, 2, 2]$
attention revolution	$[8, 4, 2]$	$[8, 4, 2]$	$[8, 4, 2]$	$[8, 4, 2]$	$[8, 4, 2]$	$[8, 4, 2]$	$[8, 4, 2]$	$[8, 4, 2]$	$[8, 4, 2]$	$[8, 4, 2]$
sampling steps	18	18	18	18	18	18	18	18	18	18

Table 14: Hyperparameter Settings for Sequence Length 96 Across Different Datasets

	ETTh1	ETTh2	ETTm1	ETTm2	Weather	Energy	Sine	Stock
General								
image size	16×16	16×16	16×16	16×16	32×32	32×32	16×16	16×16
learning rate	10^{-4}	10^{-4}	10^{-4}	10^{-4}	10^{-4}	10^{-4}	10^{-4}	10^{-4}
batch size	32	64	128	128	32	128	128	16
teacher forcing rate	0	0	0	0	0	0	0	0.2
DE								
embedding(n)	16	16	16	16	32	32	16	16
delay(m)	6	6	6	6	24	24	6	6
TST								
hidden_dim	40	40	40	40	40	40	40	40
n_heads	5	5	5	5	5	5	5	5
num_layers	6	6	6	6	6	6	6	6
Diffusion								
U-net channels	128	128	128	128	128	128	128	128
in channels	$[1, 2, 2, 2]$	$[1, 2, 2, 2]$	$[1, 2, 2, 2]$	$[1, 2, 2, 2]$	$[1, 2, 2, 4]$	$[1, 2, 2, 4]$	$[1, 2, 2, 2]$	$[1, 2, 2, 2]$
attention revolution	$[16, 8, 4, 2]$	$[16, 8, 4, 2]$	$[16, 8, 4, 2]$	$[16, 8, 4, 2]$	$[32, 16, 8, 4, 2]$	$[32, 16, 8, 4, 2]$	$[16, 8, 4, 2]$	$[16, 8, 4, 2]$
sampling steps	18	18	18	18	18	18	18	18

Table 15: Hyperparameter Settings for Sequence Length 768 Across Different Datasets

	ETTh1	ETTh2	ETTm1	ETTm2	Weather	Energy	Sine	Stock
General								
image size	32×32	32×32	32×32	32×32	32×32	32×32	32×32	32×32
learning rate	10^{-4}	10^{-4}	10^{-4}	10^{-4}	10^{-4}	10^{-4}	10^{-4}	10^{-4}
batch size	32	32	32	32	32	16	32	32
teacher forcing rate	0	0	0	0	0	0	0	0.2
DE								
embedding(n)	32	32	32	32	32	32	32	32
delay(m)	24	24	24	24	24	24	24	24
TST								
hidden_dim	40	40	40	40	40	40	40	40
n_heads	5	5	5	5	5	5	5	5
num_layers	6	6	6	6	6	6	6	6
Diffusion								
U-net channels	128	128	128	128	128	128	128	128
in channels	$[1, 2, 2, 2]$	$[1, 2, 2, 2]$	$[1, 2, 2, 2]$	$[1, 2, 2, 2]$	$[1, 2, 2, 4]$	$[1, 2, 2, 4]$	$[1, 2, 2, 2]$	$[1, 2, 2, 2]$
attention revolution	$[32, 16, 8, 4, 2]$	$[32, 16, 8, 4, 2]$	$[32, 16, 8, 4, 2]$	$[32, 16, 8, 4, 2]$	$[32, 16, 8, 4, 2]$	$[32, 16, 8, 4, 2]$	$[32, 16, 8, 4, 2]$	$[32, 16, 8, 4, 2]$
sampling steps	18	18	18	18	18	18	18	18

D.5 Natural vs. Unnatural Neighborhoods Experiment Setup

In this section, we provide a detailed explanation of the experimental setup introduced in Sec. 4.

Experiment Setup. We first generate 1000 two-dimensional samples $\{p\}$ drawn from a multivariate Gaussian distribution, with means centered at $(1, 1)$, $(1, -1)$, $(-1, 1)$, and $(-1, -1)$. A figure illustrating all sampled data appears in Figure 1A. To better simulate our real world environment, we transform each 2D datapoint into a 3×4 image by setting all pixels to zero except those at the center, which correspond to the x and y coordinates of the original point (e.g., $s[1, 1] = p[0]$ and $s[1, 2] = p[1]$). Figure 1B depicts an example of this transformation. We refer to this dataset as $\mathcal{S}_{\text{irregular}}$, as it simulates an "irregular" dataset containing zeros for missing values.

Next, we construct a second dataset, $\mathcal{S}_{\text{regular}}$, in which the zero entries are replaced with linear or nonlinear transformations of $p[0]$, $p[1]$, or both. This is intended to emulate a data-imputation step performed on the fist step of our method, yielding a more "natural" neighborhood of values. An data point example can be found in Figure 1C. We then compare three training setups:

1. Train a diffusion model to predict the score across the *entire* image (i.e., noise prediction in diffusion) on $\mathcal{S}_{\text{irregular}}$.
2. Train a diffusion model to predict *only* the two central (coordinate) pixels, using our masking technique, on $\mathcal{S}_{\text{irregular}}$.
3. Train the same masked model as in (2), but on $\mathcal{S}_{\text{regular}}$, where we have "natural neighbors."

All score models share a simple architecture: a `Conv2D` layer with a 3×4 kernel, followed by a `ReLU` activation, and a deconvolution layer that restores the original input size.

Evaluation. We employ two metrics:

1. **Score Estimation Loss:** For fair comparison, we measure the score prediction error on the two central pixels (i.e., the original coordinates), regardless of the training strategy.
2. **Kernel Analysis:** We inspect the first-layer convolution kernels to determine which pixels the model focuses on. Since there are 64 output channels, we compute the L_1 norm at each spatial position across all channels and then average them.

E Additional Experiments and Analysis

E.1 Quantitative Evaluation - Full Results

We present the complete results, including standard deviations, for the experiment conducted in the main text in Sec. 5.2. In Tab. 18, Tab. 19, and Tab. 20, we provide detailed performance results across all missing rates of 30%, 50%, and 70% for sequence lengths of 24, 96, and 768, respectively.

E.2 Qualitative Evaluation - Cont.

We provide the remaining missing rate analyses for the experiment described in Sec. 5.3. Fig. 7 presents the analysis for a 50% missing rate, while Fig. 8 shows the analysis for a 30% missing rate.

Additionally, we quantitatively assess the overlap between the original and generated data cloud points in the two-dimensional plane. We compute the Wasserstein distances between the original data and the generated samples. The results, presented in Table 16, indicate that our method consistently achieves the lowest Wasserstein distances across all missing rates and sequence lengths, outperforming KoVAE in every case. Notably, for long time series, our model exhibits significantly better performance, demonstrating its robustness in handling larger and more complex sequences with high missing rates. This underscores our approach's ability to closely match the true data distribution, even under challenging conditions, and its superior effectiveness in managing incomplete time series.

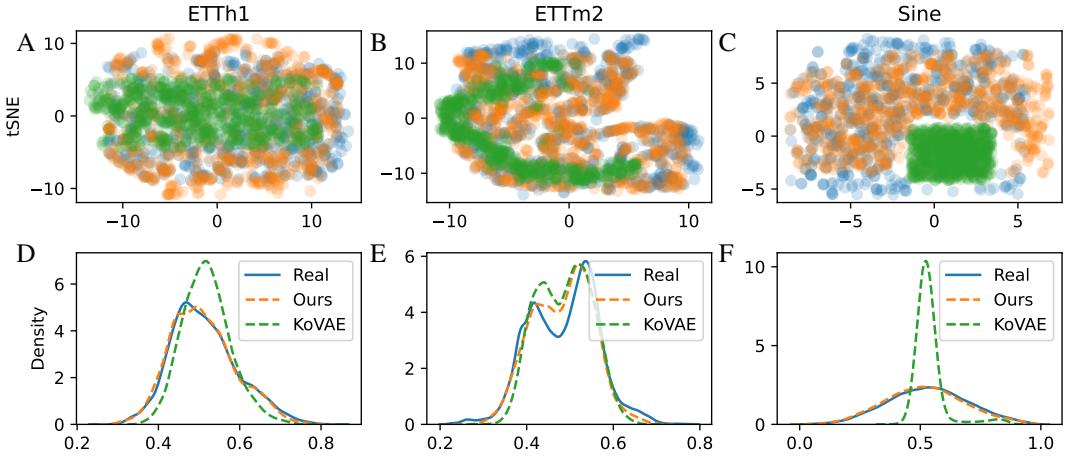

Figure 7: 2D t-SNE embeddings (top) and probability density functions (bottom) for the 50% missing rate on ETTh1 (short), ETTm2 (medium), and Sine (long) datasets.

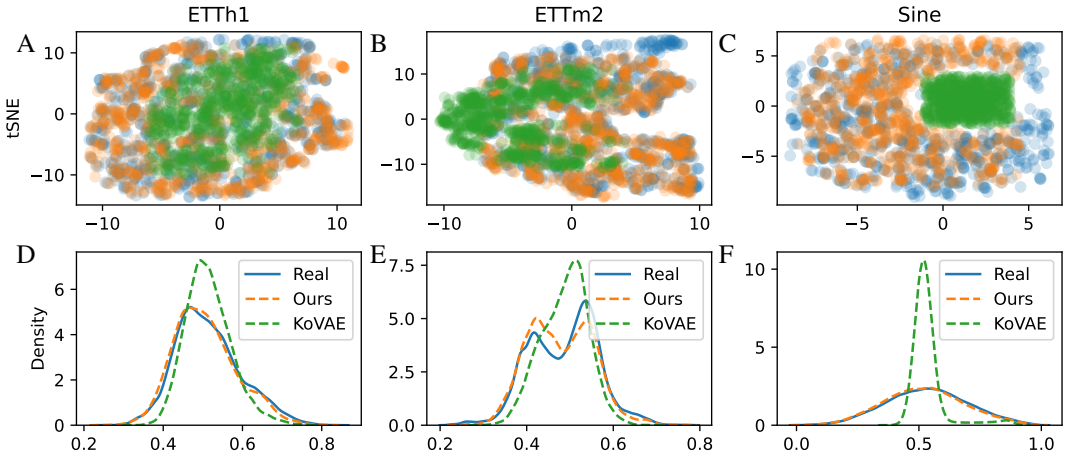

Figure 8: 2D t-SNE embeddings (top) and probability density functions (bottom) for the 30% missing rate on ETTh1 (short), ETTm2 (medium), and Sine (long) datasets.

Table 16: Wasserstein distances between original data clusters, generated samples, and clusters from KoVAE for various missing rates $(30\%, 50\%, 70\%)$ and sequence lengths. Lower values indicate better similarity.

		30% Drop			**50% Drop**			**70% Drop**		
Metric	**Model**	Energy	Weather	Stocks	ETTh1	ETTm2	Sine	ETTh1	ETTm2	Sine
Wass.↓	KoVAE	3.97	7.64	5.53	4.78	5.92	6.25	3.38	4.37	12.07
	Ours	**1.08**	**2.85**	**1.68**	**1.62**	**1.84**	**1.50**	**1.33**	**2.39**	**2.42**

E.3 Complexity Analysis Cont.

Continuing from Sec. 5.1, where we summarized the upcoming experiment, we now present the full results.

In Table 17, we report the *net* training time (in hours) for our method (**Ours**) and **KoVAE** until convergence, measured under identical hardware (RTX3090) and batch size settings. Convergence was defined by the best discriminative score achieved during training; specifically, we sampled the generated data every 10 training epochs and computed the discriminative score against the real data. Note that the times shown exclude any overhead for data generation or evaluation; we only measure the pure training runtime until the point of highest discriminative performance.

These training times are presented for three different sequence lengths (24, 96, 768) and three missing rates $(30\%, 50\%, 70\%)$. To assess the relative speedup of our approach over KoVAE, we averaged the training times of each model (when valid entries were available), computed the percentage speedup as

$$\left(\frac{\text{KoVAE time} - \text{Ours time}}{\text{KoVAE time}} \times 100\%\right),$$

and then averaged these speedups across the three missing rates. Our results show that:

- At a sequence length of 24, **Ours** converges approximately $\sim 80\%$ faster on average.
- At a sequence length of 96, **Ours** converges approximately $\sim 87\%$ faster on average.
- At a sequence length of 768, **Ours** converges approximately $\sim 85\%$ faster on average.

These figures underscore the substantial reduction in training time provided by our method, ranging from about 80% to 90% faster than KoVAE in most settings, while still achieving superior performance based on the discriminative score.

Table 17: **Training Time** (in hours) for irregular time series across sequence lengths (24, 96, 768) and missing rates (30%, 50%, 70%).

Seq. Len.	Drop %	Model	ETTh1	ETTh2	ETTm1	ETTm2	Weather	Energy	Sine	Stock
24	30%	KoVAE	5.00	15.08	11.65	7.49	9.23	12.20	5.78	2.71
		Ours	**0.73**	**0.61**	**1.18**	**0.90**	**4.77**	**2.80**	**0.50**	**0.37**
	50%	KoVAE	4.98	**4.73**	7.80	6.68	2.20	28.59	6.86	1.03
		Ours	**1.85**	6.75	**1.18**	**1.81**	**0.38**	**2.51**	**0.60**	**0.17**
	70%	KoVAE	9.45	12.55	10.98	5.48	6.08	8.91	4.22	2.36
		Ours	**1.27**	**0.92**	**0.52**	**1.58**	**5.82**	**2.02**	**0.35**	**0.08**
96	30%	KoVAE	25.80	8.10	13.79	25.92	33.87	4.94	6.90	7.71
		Ours	**3.38**	**0.80**	**1.35**	**0.95**	**2.43**	**2.36**	**1.20**	**0.23**
	50%	KoVAE	1.42	17.26	11.04	11.90	14.79	18.01	22.47	3.90
		Ours	**0.59**	**0.57**	**1.32**	**0.95**	**1.06**	**1.33**	**0.47**	**0.46**
	70%	KoVAE	31.91	7.12	19.90	15.77	17.52	18.11	2.91	7.76
		Ours	**0.61**	**4.34**	**1.05**	**3.65**	**2.12**	**1.49**	**2.72**	**1.60**
768	30%	KoVAE	62.19	59.70	92.48	69.48	40.88	13.30	18.03	16.59
		Ours	**4.72**	**1.96**	**7.57**	**6.45**	**16.46**	**3.50**	**2.93**	**3.11**
	50%	KoVAE	15.52	37.41	26.30	45.66	46.99	19.86	5.49	14.84
		Ours	**4.74**	**2.96**	**7.23**	**6.48**	**7.18**	**2.35**	**2.89**	**1.21**

Table 18: Evaluation metrics for irregular time series with 24 sequence length (30%, 50%, 70% drop). Arrows (↑ / ↓) indicate whether higher or lower values are better.

Metric	Model	Etth1	Etth2	Ettm1	Ettm2	Weather	Electricity	Energy	Sine	Stock	Mujoco
30% Drop											
Disc. ↓	TimeGAN	0.499	0.499	0.499	0.499	0.493	0.498	0.448	0.494	0.463	0.471
	GT-GAN	0.473	0.371	0.420	0.369	0.472	0.409	0.333	0.363	0.251	0.249
	KoVAE	0.208	0.075	0.045	0.077	0.229	0.497	0.280	0.035	0.162	0.123
	Ours	**0.020**	**0.009**	**0.014**	**0.006**	**0.029**	**0.399**	**0.048**	**0.013**	**0.007**	**0.009**
Pred. ↓	TimeGAN	0.156	0.305	0.146	0.262	0.388	0.183	0.375	0.145	0.087	0.118
	GT-GAN	0.174	0.092	0.119	0.097	0.147	0.148	0.066	0.099	0.021	0.048
	KoVAE	0.058	0.050	**0.044**	0.051	0.029	**0.048**	0.049	0.074	0.019	0.043
	Ours	**0.052**	**0.043**	**0.044**	**0.045**	**0.022**	**0.048**	**0.047**	**0.070**	**0.012**	**0.040**
Fid. ↓	TimeGAN	2.934	2.565	2.437	2.924	1.612	18.04	4.440	2.919	2.475	3.628
	GT-GAN	1.689	15.26	27.43	6.902	1.161	9.907	1.305	1.810	2.429	0.656
	KoVAE	1.769	0.211	0.181	0.609	0.539	7.606	0.645	0.048	0.741	0.428
	Ours	**0.071**	**0.023**	**0.023**	**0.010**	**0.018**	**3.451**	**0.033**	**0.032**	**0.009**	**0.028**
Corr. ↓	TimeGAN	6.317	0.862	2.290	0.357	0.744	11.13	3.663	2.131	0.273	0.844
	GT-GAN	7.167	0.918	2.519	0.358	0.782	14.93	3.855	3.141	0.264	0.803
	KoVAE	0.148	0.088	0.162	0.483	1.852	4.351	2.910	0.049	0.032	0.561
	Ours	**0.070**	**0.048**	**0.059**	**0.045**	**0.424**	**2.041**	**0.815**	**0.016**	**0.007**	**0.331**
50% Drop											
Disc. ↓	TimeGAN	0.499	0.499	0.499	0.499	0.499	0.498	0.479	0.496	0.487	0.483
	GT-GAN	0.462	0.371	0.407	0.376	0.496	0.391	0.317	0.372	0.265	0.270
	KoVAE	0.188	0.086	0.057	0.077	0.498	0.499	0.298	0.030	0.092	0.117
	Ours	**0.032**	**0.005**	**0.013**	**0.013**	**0.035**	**0.360**	**0.065**	**0.014**	**0.007**	**0.007**
Pred. ↓	TimeGAN	0.210	0.343	0.157	0.292	0.404	0.230	0.501	0.123	0.058	0.402
	GT-GAN	0.176	0.091	0.118	0.096	0.127	0.147	0.064	0.101	0.018	0.056
	KoVAE	0.057	0.053	0.045	0.050	0.114	**0.043**	0.050	0.072	0.019	0.042
	Ours	**0.053**	**0.045**	**0.043**	**0.041**	**0.022**	0.049	**0.047**	**0.068**	**0.012**	**0.040**
Fid. ↓	TimeGAN	4.131	3.132	2.642	2.693	2.839	20.184	6.408	2.124	2.352	4.141
	GT-GAN	1.504	5.839	4.201	9.468	5.919	9.741	1.935	1.785	2.258	0.664
	KoVAE	1.309	0.319	0.207	0.115	9.830	3.972	0.421	0.030	0.225	0.371
	Ours	**0.134**	**0.026**	**0.045**	**0.018**	**0.040**	**3.633**	**0.061**	**0.007**	**0.057**	**0.026**
Corr. ↓	TimeGAN	2.293	0.932	1.864	0.352	0.835	13.79	3.761	2.192	2.021	0.825
	GT-GAN	7.088	0.928	2.443	0.361	0.807	14.91	3.971	3.204	0.255	0.804
	KoVAE	0.173	0.283	0.132	0.157	5.027	4.152	1.822	0.029	0.072	0.555
	Ours	**0.112**	**0.047**	**0.058**	**0.026**	**0.363**	**2.044**	**0.872**	**0.015**	**0.011**	**0.342**
70% Drop											
Disc. ↓	TimeGAN	0.500	0.499	0.500	0.500	0.499	0.500	0.496	0.500	0.488	0.494
	GT-GAN	0.478	0.366	0.409	0.353	0.475	0.480	0.325	0.278	0.230	0.275
	KoVAE	0.196	0.081	0.048	0.046	0.269	0.498	0.392	0.065	0.101	0.119
	Ours	**0.058**	**0.013**	**0.010**	**0.015**	**0.106**	**0.392**	**0.128**	**0.008**	**0.010**	**0.009**
Pred. ↓	TimeGAN	0.436	0.359	0.401	0.387	0.390	0.372	0.496	0.734	0.072	0.442
	GT-GAN	0.207	0.094	0.137	0.089	0.162	0.149	0.076	0.088	0.020	0.051
	KoVAE	0.056	0.060	0.046	0.048	0.028	0.051	0.052	0.076	**0.012**	0.044
	Ours	**0.054**	**0.049**	**0.045**	**0.047**	**0.023**	**0.049**	**0.047**	**0.069**	**0.012**	**0.041**
Fid. ↓	TimeGAN	2.356	3.900	5.179	4.036	2.683	31.95	8.674	3.296	3.178	4.432
	GT-GAN	3.442	4.805	11.24	2.784	1.194	10.33	1.354	1.498	1.857	0.671
	KoVAE	1.477	0.215	0.153	0.116	0.727	7.610	0.820	0.033	0.141	0.292
	Ours	**0.167**	**0.056**	**0.073**	**0.043**	**0.451**	**3.653**	**0.301**	**0.007**	**0.041**	**0.044**
Corr. ↓	TimeGAN	6.821	0.959	2.470	0.387	0.728	14.80	3.848	3.051	3.354	0.867
	GT-GAN	7.190	0.921	2.438	0.351	0.785	14.92	3.842	3.502	0.254	0.809
	KoVAE	0.228	0.160	0.096	0.144	1.817	4.213	3.157	0.029	0.095	0.566
	Ours	**0.071**	**0.104**	**0.079**	**0.055**	**0.403**	**2.007**	**1.330**	**0.015**	**0.037**	**0.348**

Table 19: Evaluation metrics for irregular time series with 96 sequence length (30%, 50%, 70% drop). Arrows (↑ / ↓) indicate whether higher or lower values are better.

Metric	Model	Etth1	Etth2	Ettm1	Ettm2	Weather	Energy	Sine	Stock
30% Drop									
Disc. ↓	KoVAE	0.255	0.096	0.264	0.075	0.290	0.416	0.244	0.114
	Ours	**0.037**	**0.036**	**0.033**	**0.028**	**0.084**	**0.130**	**0.004**	**0.011**
Pred. ↓	KoVAE	0.062	0.062	0.053	0.047	0.040	0.077	0.164	0.016
	Ours	**0.052**	**0.045**	**0.044**	**0.042**	**0.023**	**0.048**	**0.155**	**0.010**
Fid ↓	KoVAE	5.223	0.915	4.073	0.645	2.942	4.075	2.725	0.944
	Ours	**0.156**	**0.112**	**0.147**	**0.060**	**0.169**	**0.193**	**0.018**	**0.110**
Corr. ↓	KoVAE	0.201	0.301	0.177	0.203	2.730	4.677	0.058	0.086
	Ours	**0.102**	**0.075**	**0.087**	**0.042**	**0.306**	**0.827**	**0.017**	**0.016**
50% Drop									
Disc. ↓	KoVAE	0.304	0.077	0.290	0.114	0.358	0.321	0.188	0.111
	Ours	**0.070**	**0.067**	**0.047**	**0.017**	**0.190**	**0.153**	**0.003**	**0.018**
Pred. ↓	KoVAE	0.063	0.055	0.053	0.054	0.051	0.063	0.161	0.016
	Ours	**0.054**	**0.053**	**0.044**	**0.046**	**0.025**	**0.048**	**0.155**	**0.011**
Fid ↓	KoVAE	5.370	0.781	4.663	1.325	4.117	4.955	2.334	1.003
	Ours	**0.516**	**0.487**	**0.179**	**0.130**	**0.567**	**0.182**	**0.018**	**0.105**
Corr. ↓	KoVAE	0.246	0.288	0.247	0.638	2.490	5.142	0.044	0.085
	Ours	**0.154**	**0.219**	**0.090**	**0.113**	**1.176**	**1.186**	**0.019**	**0.011**
70% Drop									
Disc. ↓	KoVAE	0.294	0.137	0.274	0.079	0.374	0.332	0.286	0.073
	Ours	**0.102**	**0.057**	**0.039**	**0.044**	**0.182**	**0.272**	**0.002**	**0.021**
Pred. ↓	KoVAE	0.062	0.055	0.056	0.049	0.047	0.064	0.171	0.029
	Ours	**0.053**	**0.050**	**0.046**	**0.044**	**0.027**	**0.051**	**0.155**	**0.012**
Fid ↓	KoVAE	6.932	1.638	3.473	1.019	3.983	5.051	8.083	0.657
	Ours	**0.399**	**0.926**	**0.187**	**0.235**	**0.447**	**0.553**	**0.016**	**0.112**
Corr. ↓	KoVAE	0.226	0.496	0.101	0.465	2.607	4.611	0.565	0.095
	Ours	**0.087**	**0.159**	**0.100**	**0.126**	**1.187**	**1.470**	**0.013**	**0.015**

Table 20: Evaluation metrics for irregular time series with 768 sequence length (30%, 50%, 70% drop). Arrows (↑ / ↓) indicate whether higher or lower values are better.

Metric	Model	Etth1	Etth2	Ettm1	Ettm2	Weather	Energy	Sine	Stock
30% Drop									
Disc. ↓	KoVAE	0.239	0.237	0.282	0.160	0.411	0.371	0.284	0.289
	Ours	**0.045**	**0.032**	**0.067**	**0.047**	**0.093**	**0.145**	**0.005**	**0.025**
Pred. ↓	KoVAE	0.077	0.074	0.059	0.081	0.061	0.089	0.223	0.020
	Ours	**0.052**	**0.056**	**0.047**	**0.051**	**0.027**	**0.025**	**0.204**	**0.011**
Fid ↓	KoVAE	11.16	9.448	11.47	8.869	12.21	25.50	38.71	7.431
	Ours	**0.318**	**0.258**	**0.373**	**0.220**	**0.110**	**0.755**	**0.184**	**0.116**
Corr. ↓	KoVAE	0.378	0.528	0.480	0.859	3.136	8.138	0.411	0.041
	Ours	**0.088**	**0.119**	**0.126**	**0.086**	**0.269**	**0.849**	**0.006**	**0.004**
50% Drop									
Disc. ↓	KoVAE	0.270	0.191	0.197	0.225	0.428	0.372	0.426	0.302
	Ours	**0.061**	**0.030**	**0.061**	**0.048**	**0.097**	**0.244**	**0.009**	**0.029**
Pred. ↓	KoVAE	0.074	0.064	0.056	0.084	0.064	0.086	0.222	0.023
	Ours	**0.053**	**0.057**	**0.047**	**0.048**	**0.027**	**0.051**	**0.204**	**0.015**
Fid ↓	KoVAE	14.56	7.412	11.51	9.373	18.59	19.58	38.49	8.274
	Ours	**0.589**	**0.248**	**0.305**	**0.211**	**0.225**	**0.916**	**0.211**	**0.199**
Corr. ↓	KoVAE	0.290	0.574	0.428	0.842	4.836	12.63	0.336	0.085
	Ours	**0.103**	**0.128**	**0.107**	**0.119**	**0.455**	**1.473**	**0.006**	**0.042**
70% Drop									
Disc. ↓	KoVAE	0.206	0.176	0.231	0.203	0.445	0.409	0.340	0.263
	Ours	**0.160**	**0.072**	**0.046**	**0.061**	**0.116**	**0.251**	**0.005**	**0.013**
Pred. ↓	KoVAE	0.065	0.071	0.065	0.062	0.086	0.088	0.234	0.051
	Ours	**0.054**	**0.056**	**0.047**	**0.052**	**0.028**	**0.050**	**0.204**	**0.013**
Fid ↓	KoVAE	16.05	8.052	17.54	6.595	21.69	28.46	38.60	6.114
	Ours	**1.739**	**0.812**	**0.496**	**0.362**	**0.619**	**0.718**	**0.317**	**0.167**
Corr. ↓	KoVAE	0.331	0.718	0.305	0.515	1.786	5.49	0.391	**0.013**
	Ours	**0.118**	**0.071**	**0.133**	**0.179**	**0.650**	**0.798**	**0.006**	0.034

NeurIPS Paper Checklist

The checklist is designed to encourage best practices for responsible machine learning research, addressing issues of reproducibility, transparency, research ethics, and societal impact. Do not remove the checklist: **The papers not including the checklist will be desk rejected.** The checklist should follow the references and follow the (optional) supplemental material. The checklist does NOT count towards the page limit.

Please read the checklist guidelines carefully for information on how to answer these questions. For each question in the checklist:

- You should answer [Yes] , [No] , or [NA] .
- [NA] means either that the question is Not Applicable for that particular paper or the relevant information is Not Available.
- Please provide a short (1–2 sentence) justification right after your answer (even for NA).

The checklist answers are an integral part of your paper submission. They are visible to the reviewers, area chairs, senior area chairs, and ethics reviewers. You will be asked to also include it (after eventual revisions) with the final version of your paper, and its final version will be published with the paper.

The reviewers of your paper will be asked to use the checklist as one of the factors in their evaluation. While "[Yes] " is generally preferable to "[No] ", it is perfectly acceptable to answer "[No] " provided a proper justification is given (e.g., "error bars are not reported because it would be too computationally expensive" or "we were unable to find the license for the dataset we used"). In general, answering "[No] " or "[NA] " is not grounds for rejection. While the questions are phrased in a binary way, we acknowledge that the true answer is often more nuanced, so please just use your best judgment and write a justification to elaborate. All supporting evidence can appear either in the main paper or the supplemental material, provided in appendix. If you answer [Yes] to a question, in the justification please point to the section(s) where related material for the question can be found.

IMPORTANT, please:

- **Delete this instruction block, but keep the section heading "NeurIPS Paper Checklist"**,
- **Keep the checklist subsection headings, questions/answers and guidelines below.**
- **Do not modify the questions and only use the provided macros for your answers**.

1. **Claims**

   Question: Do the main claims made in the abstract and introduction accurately reflect the paper's contributions and scope?

   Answer: [Yes]

   Justification: The abstract and introduction clearly outline the problem of generating regular time series from irregular data and present the two-step method (completion + masking), which is consistently analyzed throughout the paper (see Abstract, Sec. 1, Sec. 4, and Sec. 5).

   Guidelines:

   - The answer NA means that the abstract and introduction do not include the claims made in the paper.
   - The abstract and/or introduction should clearly state the claims made, including the contributions made in the paper and important assumptions and limitations. A No or NA answer to this question will not be perceived well by the reviewers.
   - The claims made should match theoretical and experimental results, and reflect how much the results can be expected to generalize to other settings.
   - It is fine to include aspirational goals as motivation as long as it is clear that these goals are not attained by the paper.

2. **Limitations**

   Question: Does the paper discuss the limitations of the work performed by the authors?

   Answer: [Yes]

Justification: The paper discusses the limitations of naive masking and inverse transformations in Sec. 4, and includes ablation studies in Sec. 5.7 to analyze failure cases and model sensitivity.

Guidelines:

- The answer NA means that the paper has no limitation while the answer No means that the paper has limitations, but those are not discussed in the paper.
- The authors are encouraged to create a separate "Limitations" section in their paper.
- The paper should point out any strong assumptions and how robust the results are to violations of these assumptions (e.g., independence assumptions, noiseless settings, model well-specification, asymptotic approximations only holding locally). The authors should reflect on how these assumptions might be violated in practice and what the implications would be.
- The authors should reflect on the scope of the claims made, e.g., if the approach was only tested on a few datasets or with a few runs. In general, empirical results often depend on implicit assumptions, which should be articulated.
- The authors should reflect on the factors that influence the performance of the approach. For example, a facial recognition algorithm may perform poorly when image resolution is low or images are taken in low lighting. Or a speech-to-text system might not be used reliably to provide closed captions for online lectures because it fails to handle technical jargon.
- The authors should discuss the computational efficiency of the proposed algorithms and how they scale with dataset size.
- If applicable, the authors should discuss possible limitations of their approach to address problems of privacy and fairness.
- While the authors might fear that complete honesty about limitations might be used by reviewers as grounds for rejection, a worse outcome might be that reviewers discover limitations that aren't acknowledged in the paper. The authors should use their best judgment and recognize that individual actions in favor of transparency play an important role in developing norms that preserve the integrity of the community. Reviewers will be specifically instructed to not penalize honesty concerning limitations.

3. **Theory assumptions and proofs**

   Question: For each theoretical result, does the paper provide the full set of assumptions and a complete (and correct) proof?

   Answer: [NA]

   Justification: The paper does not include theoretical results or formal theorems—it is an empirical study focused on generative modeling and experimental evaluation.

   Guidelines:

   - The answer NA means that the paper does not include theoretical results.
   - All the theorems, formulas, and proofs in the paper should be numbered and cross-referenced.
   - All assumptions should be clearly stated or referenced in the statement of any theorems.
   - The proofs can either appear in the main paper or the supplemental material, but if they appear in the supplemental material, the authors are encouraged to provide a short proof sketch to provide intuition.
   - Inversely, any informal proof provided in the core of the paper should be complemented by formal proofs provided in appendix or supplemental material.
   - Theorems and Lemmas that the proof relies upon should be properly referenced.

4. **Experimental result reproducibility**

   Question: Does the paper fully disclose all the information needed to reproduce the main experimental results of the paper to the extent that it affects the main claims and/or conclusions of the paper (regardless of whether the code and data are provided or not)?

   Answer: [Yes]

Justification: The paper provides extensive implementation details including training parameters, model architecture (Sec. 4, App. B, and hyperparameter tables in the appendix), datasets used, evaluation metrics, and ablation studies.

Guidelines:

- The answer NA means that the paper does not include experiments.
- If the paper includes experiments, a No answer to this question will not be perceived well by the reviewers: Making the paper reproducible is important, regardless of whether the code and data are provided or not.
- If the contribution is a dataset and/or model, the authors should describe the steps taken to make their results reproducible or verifiable.
- Depending on the contribution, reproducibility can be accomplished in various ways. For example, if the contribution is a novel architecture, describing the architecture fully might suffice, or if the contribution is a specific model and empirical evaluation, it may be necessary to either make it possible for others to replicate the model with the same dataset, or provide access to the model. In general. releasing code and data is often one good way to accomplish this, but reproducibility can also be provided via detailed instructions for how to replicate the results, access to a hosted model (e.g., in the case of a large language model), releasing of a model checkpoint, or other means that are appropriate to the research performed.
- While NeurIPS does not require releasing code, the conference does require all submissions to provide some reasonable avenue for reproducibility, which may depend on the nature of the contribution. For example
  (a) If the contribution is primarily a new algorithm, the paper should make it clear how to reproduce that algorithm.
  (b) If the contribution is primarily a new model architecture, the paper should describe the architecture clearly and fully.
  (c) If the contribution is a new model (e.g., a large language model), then there should either be a way to access this model for reproducing the results or a way to reproduce the model (e.g., with an open-source dataset or instructions for how to construct the dataset).
  (d) We recognize that reproducibility may be tricky in some cases, in which case authors are welcome to describe the particular way they provide for reproducibility. In the case of closed-source models, it may be that access to the model is limited in some way (e.g., to registered users), but it should be possible for other researchers to have some path to reproducing or verifying the results.

5. **Open access to data and code**

   Question: Does the paper provide open access to the data and code, with sufficient instructions to faithfully reproduce the main experimental results, as described in supplemental material?

   Answer: [No]

   Justification: Code and data will be released after the review process concludes (post-acceptance or rejection), as noted by the authors.

   Guidelines:

   - The answer NA means that paper does not include experiments requiring code.
   - Please see the NeurIPS code and data submission guidelines (`https://nips.cc/public/guides/CodeSubmissionPolicy`) for more details.
   - While we encourage the release of code and data, we understand that this might not be possible, so "No" is an acceptable answer. Papers cannot be rejected simply for not including code, unless this is central to the contribution (e.g., for a new open-source benchmark).
   - The instructions should contain the exact command and environment needed to run to reproduce the results. See the NeurIPS code and data submission guidelines (`https://nips.cc/public/guides/CodeSubmissionPolicy`) for more details.
   - The authors should provide instructions on data access and preparation, including how to access the raw data, preprocessed data, intermediate data, and generated data, etc.

- The authors should provide scripts to reproduce all experimental results for the new proposed method and baselines. If only a subset of experiments are reproducible, they should state which ones are omitted from the script and why.
- At submission time, to preserve anonymity, the authors should release anonymized versions (if applicable).
- Providing as much information as possible in supplemental material (appended to the paper) is recommended, but including URLs to data and code is permitted.

6. **Experimental setting/details**

   Question: Does the paper specify all the training and test details (e.g., data splits, hyperparameters, how they were chosen, type of optimizer, etc.) necessary to understand the results?

   Answer: [Yes]

   Justification: Training/test splits, hyperparameters, sampling steps, and optimizer settings are provided in Sec. 5 and in App. D.3, Tables 13–15.

   Guidelines:

   - The answer NA means that the paper does not include experiments.
   - The experimental setting should be presented in the core of the paper to a level of detail that is necessary to appreciate the results and make sense of them.
   - The full details can be provided either with the code, in appendix, or as supplemental material.

7. **Experiment statistical significance**

   Question: Does the paper report error bars suitably and correctly defined or other appropriate information about the statistical significance of the experiments?

   Answer: [Yes]

   Justification: The paper provides average results over multiple random seeds and missing rates (e.g., 30%, 50%, 70%), and includes standard deviation in extended tables in the appendix (e.g., Tab. 18, Tab. 20).

   Guidelines:

   - The answer NA means that the paper does not include experiments.
   - The authors should answer "Yes" if the results are accompanied by error bars, confidence intervals, or statistical significance tests, at least for the experiments that support the main claims of the paper.
   - The factors of variability that the error bars are capturing should be clearly stated (for example, train/test split, initialization, random drawing of some parameter, or overall run with given experimental conditions).
   - The method for calculating the error bars should be explained (closed form formula, call to a library function, bootstrap, etc.)
   - The assumptions made should be given (e.g., Normally distributed errors).
   - It should be clear whether the error bar is the standard deviation or the standard error of the mean.
   - It is OK to report 1-sigma error bars, but one should state it. The authors should preferably report a 2-sigma error bar than state that they have a 96% CI, if the hypothesis of Normality of errors is not verified.
   - For asymmetric distributions, the authors should be careful not to show in tables or figures symmetric error bars that would yield results that are out of range (e.g. negative error rates).
   - If error bars are reported in tables or plots, The authors should explain in the text how they were calculated and reference the corresponding figures or tables in the text.

8. **Experiments compute resources**

   Question: For each experiment, does the paper provide sufficient information on the computer resources (type of compute workers, memory, time of execution) needed to reproduce the experiments?

Answer: [Yes]

Justification: Training and inference times are detailed and compared to baselines in Sec. 5.1 and App. E.3, with hardware specs (e.g., RTX3090) provided for fair benchmarking.

Guidelines:

- The answer NA means that the paper does not include experiments.
- The paper should indicate the type of compute workers CPU or GPU, internal cluster, or cloud provider, including relevant memory and storage.
- The paper should provide the amount of compute required for each of the individual experimental runs as well as estimate the total compute.
- The paper should disclose whether the full research project required more compute than the experiments reported in the paper (e.g., preliminary or failed experiments that didn't make it into the paper).

9. **Code of ethics**

Question: Does the research conducted in the paper conform, in every respect, with the NeurIPS Code of Ethics `https://neurips.cc/public/EthicsGuidelines`?

Answer: [Yes]

Justification: The paper does not raise ethical concerns; all datasets are public, and the work does not involve sensitive data or human participants.

Guidelines:

- The answer NA means that the authors have not reviewed the NeurIPS Code of Ethics.
- If the authors answer No, they should explain the special circumstances that require a deviation from the Code of Ethics.
- The authors should make sure to preserve anonymity (e.g., if there is a special consideration due to laws or regulations in their jurisdiction).

10. **Broader impacts**

Question: Does the paper discuss both potential positive societal impacts and negative societal impacts of the work performed?

Answer: [Yes]

Justification: The paper highlights potential applications in healthcare, finance, and climate science (see Abstract and Sec. 1), and discusses risks related to data imputation and overreliance on incorrect completions (Sec. 4).

Guidelines:

- The answer NA means that there is no societal impact of the work performed.
- If the authors answer NA or No, they should explain why their work has no societal impact or why the paper does not address societal impact.
- Examples of negative societal impacts include potential malicious or unintended uses (e.g., disinformation, generating fake profiles, surveillance), fairness considerations (e.g., deployment of technologies that could make decisions that unfairly impact specific groups), privacy considerations, and security considerations.
- The conference expects that many papers will be foundational research and not tied to particular applications, let alone deployments. However, if there is a direct path to any negative applications, the authors should point it out. For example, it is legitimate to point out that an improvement in the quality of generative models could be used to generate deepfakes for disinformation. On the other hand, it is not needed to point out that a generic algorithm for optimizing neural networks could enable people to train models that generate Deepfakes faster.
- The authors should consider possible harms that could arise when the technology is being used as intended and functioning correctly, harms that could arise when the technology is being used as intended but gives incorrect results, and harms following from (intentional or unintentional) misuse of the technology.

- If there are negative societal impacts, the authors could also discuss possible mitigation strategies (e.g., gated release of models, providing defenses in addition to attacks, mechanisms for monitoring misuse, mechanisms to monitor how a system learns from feedback over time, improving the efficiency and accessibility of ML).

11. **Safeguards**

    Question: Does the paper describe safeguards that have been put in place for responsible release of data or models that have a high risk for misuse (e.g., pretrained language models, image generators, or scraped datasets)?

    Answer: [NA]

    Justification: The paper does not release a general-purpose model or scraped dataset and poses no high risk for misuse.

    Guidelines:

    - The answer NA means that the paper poses no such risks.
    - Released models that have a high risk for misuse or dual-use should be released with necessary safeguards to allow for controlled use of the model, for example by requiring that users adhere to usage guidelines or restrictions to access the model or implementing safety filters.
    - Datasets that have been scraped from the Internet could pose safety risks. The authors should describe how they avoided releasing unsafe images.
    - We recognize that providing effective safeguards is challenging, and many papers do not require this, but we encourage authors to take this into account and make a best faith effort.

12. **Licenses for existing assets**

    Question: Are the creators or original owners of assets (e.g., code, data, models), used in the paper, properly credited and are the license and terms of use explicitly mentioned and properly respected?

    Answer: [Yes]

    Justification: All datasets used are public and cited correctly (e.g., UCI, ETT, USHCN); the codebases cited are academic open-source projects (e.g., TS2Vec, ImagenTime).

    Guidelines:

    - The answer NA means that the paper does not use existing assets.
    - The authors should cite the original paper that produced the code package or dataset.
    - The authors should state which version of the asset is used and, if possible, include a URL.
    - The name of the license (e.g., CC-BY 4.0) should be included for each asset.
    - For scraped data from a particular source (e.g., website), the copyright and terms of service of that source should be provided.
    - If assets are released, the license, copyright information, and terms of use in the package should be provided. For popular datasets, `paperswithcode.com/datasets` has curated licenses for some datasets. Their licensing guide can help determine the license of a dataset.
    - For existing datasets that are re-packaged, both the original license and the license of the derived asset (if it has changed) should be provided.
    - If this information is not available online, the authors are encouraged to reach out to the asset's creators.

13. **New assets**

    Question: Are new assets introduced in the paper well documented and is the documentation provided alongside the assets?

    Answer: [NA]

    Justification: Although the paper proposes a new model architecture, no new dataset or code repository is released at submission time; these will be released post-review.

    Guidelines:

- The answer NA means that the paper does not release new assets.
- Researchers should communicate the details of the dataset/code/model as part of their submissions via structured templates. This includes details about training, license, limitations, etc.
- The paper should discuss whether and how consent was obtained from people whose asset is used.
- At submission time, remember to anonymize your assets (if applicable). You can either create an anonymized URL or include an anonymized zip file.

14. **Crowdsourcing and research with human subjects**

    Question: For crowdsourcing experiments and research with human subjects, does the paper include the full text of instructions given to participants and screenshots, if applicable, as well as details about compensation (if any)?

    Answer: [NA]

    Justification: The paper does not involve crowdsourcing or human subjects.

    Guidelines:

    - The answer NA means that the paper does not involve crowdsourcing nor research with human subjects.
    - Including this information in the supplemental material is fine, but if the main contribution of the paper involves human subjects, then as much detail as possible should be included in the main paper.
    - According to the NeurIPS Code of Ethics, workers involved in data collection, curation, or other labor should be paid at least the minimum wage in the country of the data collector.

15. **Institutional review board (IRB) approvals or equivalent for research with human subjects**

    Question: Does the paper describe potential risks incurred by study participants, whether such risks were disclosed to the subjects, and whether Institutional Review Board (IRB) approvals (or an equivalent approval/review based on the requirements of your country or institution) were obtained?

    Answer: [NA]

    Justification: The paper does not involve human participants and does not require IRB approval.

    Guidelines:

    - The answer NA means that the paper does not involve crowdsourcing nor research with human subjects.
    - Depending on the country in which research is conducted, IRB approval (or equivalent) may be required for any human subjects research. If you obtained IRB approval, you should clearly state this in the paper.
    - We recognize that the procedures for this may vary significantly between institutions and locations, and we expect authors to adhere to the NeurIPS Code of Ethics and the guidelines for their institution.
    - For initial submissions, do not include any information that would break anonymity (if applicable), such as the institution conducting the review.

16. **Declaration of LLM usage**

    Question: Does the paper describe the usage of LLMs if it is an important, original, or non-standard component of the core methods in this research? Note that if the LLM is used only for writing, editing, or formatting purposes and does not impact the core methodology, scientific rigorousness, or originality of the research, declaration is not required.

    Answer: [NA]

    Justification: LLMs were not used in the methodology, only lightly for text editing and formatting.

    Guidelines:

- The answer NA means that the core method development in this research does not involve LLMs as any important, original, or non-standard components.
- Please refer to our LLM policy (`https://neurips.cc/Conferences/2025/LLM`) for what should or should not be described.